JOURNAL OF GLACIOLOGY

CAMBRIDGE UNIVERSITY PRESS



# Surging vs. streaming: the dual fast ice flow response to variations in efficiency of the subglacial drainage landsystem

| | |
|---|---|
| Journal: | *Journal of Glaciology* |
| Manuscript ID | Draft |
| Manuscript Type: | Article |
| Date Submitted by the Author: | n/a |
| Complete List of Authors: | Ravier, Edouard; LPG,<br>Lelandais, Thomas; LPG<br>Vérité, Jean; LPG<br>Bourgeois, Olivier; LPG |
| Keywords: | Glacial geomorphology, Ice streams, Glacier surges, Glacier hydrology, Glaciological model experiments |
| Abstract: | Observation and modelling have long contributed to associate surging and streaming of glaciers with glacier thermal regime, variations in meltwater availability and pressure and mechanical coupling at their beds. Using experimental modelling and palaeoglaciological mapping, we explore how the development of subglacial drainage landsystems controls variations in drainage efficiency and ice flow velocities for terrestrial-based ice lobes on flat horizontal beds. We observe that the achievement or not of efficient subglacial drainage landsystems determines the fast-flow regime of these glaciers. In the surge regime, |

| | |
|---|---|
| | rapid increase of drainage efficiency through development of tunnel valleys and their tributaries reduces the duration of ice flow speed-up events by lowering water pressures and increasing ice-bed coupling. Tunnel valleys connected to ice lobe margins, submarginal thrust moraines, reduced ice lobe extensions and ephemeral shear margins are the most distinctive characteristics of this regime. In the stream regime, disconnected channels of smaller dimensions develop, but they are unable to evacuate all the meltwater: this prolonged drainage inefficiency leads to sustained high ice flow velocity and steady shear margins. Small and rectilinear meltwater channels devoid of tributaries, often disconnected from ice lobe margins and lineation swarms are diagnostic of this regime. |
| | |

# Surging vs. streaming: the dual fast ice flow response to variations in efficiency of the subglacial drainage landsystem

Édouard Ravier[1], Thomas Lelandais[1], Jean Vérité[1], Olivier Bourgeois[2]

*[1] Laboratoire de Planétologie et Géosciences, UMR 6112, CNRS, Le Mans Université, Avenue Olivier Messiaen, 72085 Le Mans CEDEX 9, France*

*[2] Laboratoire de Planétologie et Géosciences, UMR 6112, CNRS, Nantes Université, 2 rue de la Houssinière, BP 92208, 44322 Nantes CEDEX 3, France*

**Keywords :** Ice Surge ; Ice stream ; drainage efficiency ; experimental modelling; palaeoglaciology

## Abstract

Observation and modelling have long contributed to associate surging and streaming of glaciers with glacier thermal regime, variations in meltwater availability and pressure and mechanical coupling at their beds. Using experimental modelling and palaeoglaciological mapping, we explore how the development of subglacial drainage landsystems controls variations in drainage efficiency and ice flow velocities for terrestrial-based ice lobes on flat horizontal beds. We observe that the achievement or not of efficient subglacial drainage landsystems determines the fast-flow regime of these glaciers. In the surge regime, rapid increase of drainage efficiency through development of tunnel valleys and their tributaries reduces the duration of ice flow speed-up events by lowering water pressures and increasing ice-bed coupling. Tunnel valleys connected to ice lobe margins, submarginal thrust moraines, reduced ice lobe extensions and ephemeral shear margins are the most distinctive characteristics of this regime. In the stream regime, disconnected channels of smaller dimensions develop, but they are unable to evacuate all the meltwater: this prolonged drainage inefficiency leads to sustained high ice flow velocity and steady shear margins. Small and rectilinear meltwater channels devoid of tributaries, often disconnected from ice lobe margins and lineation swarms are diagnostic of this regime.

## 1. INTRODUCTION

The magnitude and duration of fast ice b flow events control the transfer rate of ice from interiors to margins of ice sheets, thus influencing their mass balances (Rignot and others, 2019; Mouginot and others, 2019), potentially raising sea level for marine-based ice streams (Zemp and others, 2019) and controlling the dynamics of ice lobes for their terrestrial counterparts (Patterson, 1997; Jennings, 2006). Fast-flow events can consist in either monthly to yearly cyclic ice speed-up events, referred to as surges, or sustained fast-flow along ice streams over decades to centuries, with potential switches from surge- to stream-like flow regimes (Zheng and others, 2019). A relationship between the efficiency of subglacial meltwater drainage and fast-flow regimes has been now established from various investigation methods: tracer experiments, numerical modelling, physical modelling, palaeoglaciological mapping, ground penetrating radar and seismic monitoring (Chandler and others, 2013, 2021; Lelandais and others, 2018; Davison and others, 2020; Nanni and others, 2021; Pitcher and others, 2020). Theories of surging and streaming must therefore address the issue of drainage system evolution due to its strong potential to modulate the response of the most dynamics glacier outlets to climate warming (Kamb and others, 1985; Fowler, 1987; Elsworth and Suckale, 2016. Lelandais and others, 2018; Benn and others, 2019).

Variations in drainage efficiency, by affecting basal lubrication and subglacial pressure, are critical to understand the origin and duration of fast ice flow events (Zwally and others, 2002; Das and others, 2008; Joughin and others, 2008; Palmer and others, 2011; Fitzpatrick and others, 2013). The drainage efficiency is the potential rate of meltwater transfer in the subglacial drainage system; as such, it controls the balance between meltwater supply, storage and discharge. It depends mostly on the bed topography, the bed materials, the thickness, temperature and surface gradient of the ice and the rate and distribution of meltwater flow to the bed (Fountain and Walder, 1998). Under efficient drainage, all meltwater is routed and transferred to the margin through passageways without causing significant increase of subglacial water pressure (Chandler and others, 2021). Under inefficient drainage, the capacity of meltwater transfer is reduced, resulting in higher subglacial water pressure. These two drainage configurations are usually distinguished by the shape and spatial distribution of their subglacial passageways and thus the ease of meltwater to flow (Nienow and others, 2017). Various kinds of meltwater passageways have been recognized over the years and have been generally classified in two categories, respectively associated with (i) "efficient" drainage also referred to "channelised" "fast" or "low-pressure" drainage and (ii) "inefficient" drainage also referred to as "distributed" or "slow" or high-pressure" drainage (Flowers, 2015). Drainage elements classically associated with efficient drainage include conduits cut either up into the ice (Röthlisberger channel) or down into the bed (Nye channel; meltwater channels, tunnel valleys) (e.g. Rothlisberger, 1972; Shreve, 1972; Nye,1973; Hooke and others, 1990). Drainage elements revealing inefficient drainage are classically characterised either by water films, linked cavities, braided canals or groundwater flows (Lliboutry, 1968; Weertman, 1972; Walder, 1986; Kamb, 1987; Walder and Fowler, 1994; Boulton and others, 1995).

The subglacial hydrological system and its associated landsystem imprint are increasingly prone to reorganization related to changing discharge and evolution of both drainage efficiency and connectivity (Bell, 2008; Bartholomew and others, 2012; Sundal and others, 2011; Andrews and others, 2014; Davison and others, 2019).The ability of the subglacial drainage landsystem to evolve morphologically, thus to display spatial and temporal transitions between efficient and inefficient drainages, modulates the ice flow dynamics. Efficient drainage characterised by channelised and connected passageways is usually associated with reduced ice flow velocities, while inefficient distributed drainage is commonly associated with flow speed-up (Lliboutry, 1968; Bindschadler, 1983;

Hewitt, 2011; Tedstone and others, 2015; Davison and others, 2019), with possible switches from one regime to another at seasonal to decadal timescales.

When, where and how subglacial water drainage enhances or impedes glacier flow is poorly-constrained however, due to the paucity of direct observations of subglacial drainage characteristics. Reorganisation of the subglacial hydrology and its impact on ice flow velocity have mainly been monitored at daily, monthly or seasonal time scales on modern glacier systems (Iken and Bindschadler, 1986, Vijay and others, 2021; Davison and others, 2020), but the hydrological response at longer timescales (i.e., deglaciation timescale) has not been explored. Current models do not capture all relevant feedbacks between water drainage, subglacial landscape development and ice dynamics to predict long-term trends in glacial flow. Subglacial landscapes exposed in formerly glaciated areas include palaeo-drainage networks that potentially record decadal to centennial timespans of subglacial drainage system evolution and offer a large-scale window in hydrological processes otherwise difficult to observe beneath contemporary ice masses (Brennand, 2000; Livingstone and others, 2017; Ahokangas and others, 2021). By fossilizing the final evolution of subglacial drainage landsystems developed during the decay of ice sheets, meltwater landforms including tunnel valleys, meltwater channels and eskers provide inspiring models for the geometry, efficiency and development of subglacial drainage systems (Kehew and others, 1999; Storrar and others, 2014; Lewington and others, 2020; Sharpe and others, 2021). Physical experiments have recently contributed to conceptualise the relationship between subglacial hydrology, ice flow dynamics and shaping of subglacial landsystems by modelling the processes responsible for the development of channelised water passageways (tunnel valleys) and landforms (fans, ribbed bedforms, murtoos) (Lelandais and others, 2016, 2018; Vérité and others, 2021, 2022).

To better constrain the role of changes in morphology and efficiency of subglacial drainage landsystems on the behavior and duration of fast ice flow events at land-terminating glacier margins, we combine (i) monitoring of drainage evolution and ice dynamics in an experimental model of pressurized hydrological systems and (ii) detailed examination of drainage networks and associated landform signatures for two neighboring palaeo-ice lobes of the Laurentide Ice Sheet (northwest, territories, Great Slave Lake Ice Stream).

## 2. EXPERIMENTAL MODELLING

### 2.1 Methods

#### *2.1.1. Experimental setup and scenario*

The experimental method and scaling is fully described in Lelandais and others (2016, 2018). The model is set in a glass box (70 cm long, 70 cm wide and 5 cm deep) (**Fig. 1A**). A 5 cm thick, flat, horizontal, permeable and erodible bed, made of sand ($d_{50}$=100 µm) saturated with pure water and compacted to ensure homogeneous values for its density ($\rho_{bulk} = 2000$ kg.m$^{-3}$), porosity ($\Phi = 41$ %) and permeability ($K = 10^{-4}$ m.s$^{-1}$), rests on the box floor. The ice sheet portion is modelled with a 3 centimeter-thick cap of viscous ($\eta = 5{\cdot}10^4$ Pa.s$^{-}$) and transparent but refractive ($n = 1.47$) silicone putty placed on the bed (**Fig. 1B**). The silicone cap is circular in top view to avoid lateral boundary effects and 15 cm in radius at the onset of the experiments. Subglacial meltwater production is simulated by injection of water with a pump (**Fig. 1B**). The injector is placed at a depth of 1.8 cm in the bed below the centre of the silicone cap. During the experiment, the water discharge generates a water flow within the bed and at the silicone-bed interface. Once injected, water flow occurs as darcian flow within the bed and interfacial flow at the silicone–bed contact. The water flowing at the silicone–bed interface originates from a pipe that forms in the bed above the injector, once the water pressure has exceeded the cumulative pressure of the silicone and sand layers. The ratio between darcian and interfacial flows, as computed from the input discharge, the water discharge through the pipe and the bed permeability, is on the order of 3 (Lelandais, 2018).

We performed 24 experiments with constant water discharge ($3.10^{-7}$m$^3$.s$^{-1}$) during 30 min. They produced two types of drainage landsystems and silicone flow regimes. The results of two typical experiments (n° 2 and 21; **Table S1**), representative of these regimes, are shown in **Figures 2** and **4**. The results of the other experiments are compiled and averaged in **Table 1**.

*2.1.2. Monitoring*

Monitoring of the experiments is achieved by means of seven synchronized cameras to ensure the production of time series silicone flow velocity maps and Digitial Elevation Models (DEMs) (**Fig. 1A**). Photogrammetry is used to build DEMs of the silicone surface and silicone-bed interface (Lelandais and others, 2016, 2018). Morphological parameters (width, depth, length and sinuosity) are extracted for any single drainage element from these DEMs.

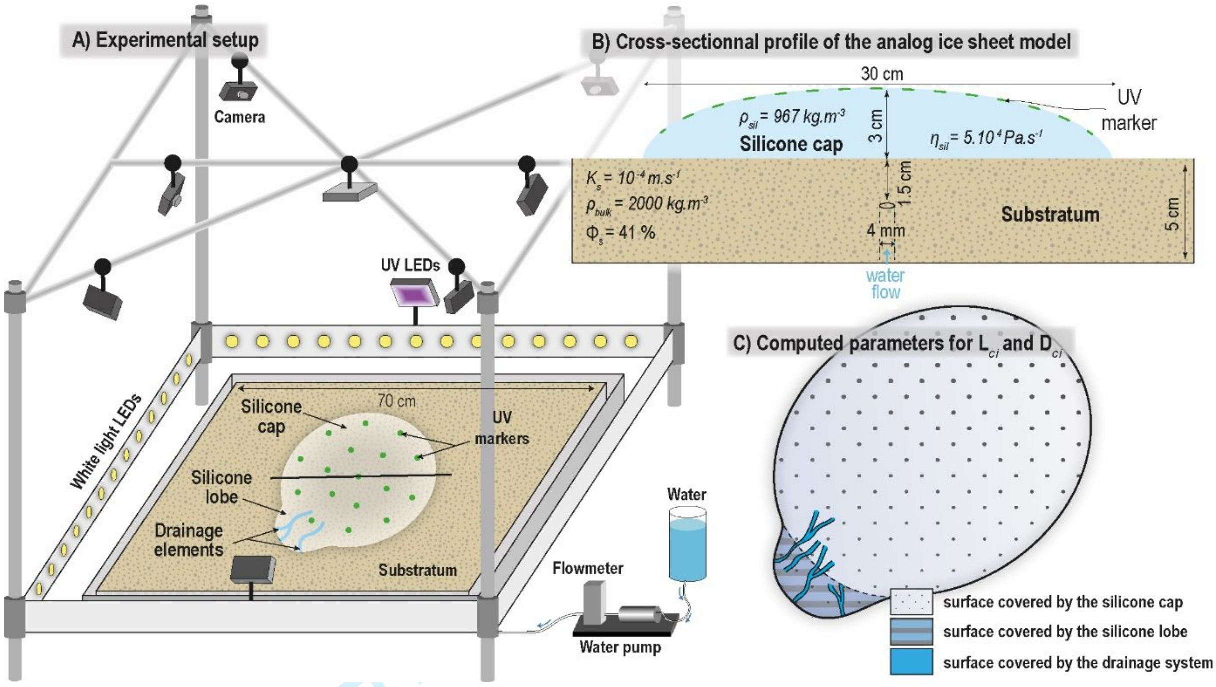


***Figure 1.*** *Description of the experimental device (after Lelandais and others, 2018) with (A) a setup overview showing the injection apparatus and the monitoring system and (B) a cross-sectional profile of the analog device displaying the position of UV markers and the physical characteristics of both the bed and the silicone cap. Parameters measured to compute the lobe cover index (Lci) and the drainage cover index (Dci) is presented in (C).*

The displacement of punctual UV markers scattered at the silicone surface is monitored by a central camera, allowing the silicone flow velocity to be determined using particle image velocimetry techniques (**Fig. 1A**). The horizontal deformation of the silicone cap surface is quantified by measuring the magnitude of the horizontal shear strain rate ($\varepsilon_{shear}$; Nye, 1959). Those indicators are computed for each triangle of a mesh, established by a Delaunay triangulation of all the UV markers following methods developed by Vérité and others (2021). Simultaneous monitoring of subglacial drainage landforms, silicone flow velocity and silicon deformation allows connections between the subsilicone drainage system and silicone dynamics evolution to be analysed (Lelandais and others, 2018).

In order to correlate water flow, morphological changes of the bed and silicone dynamics, we compute from the time series DEMs the maximal discharge capacity the drainage elements are able to accommodate. We use the Poiseuille law (**1**), which connects the hydraulic radius (Rh) of a drainage element, its length (L), the water viscosity (η) and the water pressure gradient (ΔP) through the drainage element to the maximal discharge ($Qmax_{element}$) the element is able to drain when considered at bankfull state. The hydraulic radius is taken as the ratio between the area (A) and perimeter (P) of the drainage element cross-sections.

$$(1)\ Qmax_{element} = \frac{\Delta P\ \pi\ Rh^4}{8\eta\ L} \text{ with } Rh = \frac{A}{P}$$

$$(2)\ Qmax_{system} = \sum Qmax_{element}$$

By summing maximal discharge capacities of all observed drainage elements, we compute the maximal discharge capacity of the whole drainage landsystem ($Qmax_{element}$) (**2**). To monitor drainage efficiency through time, we compare $Qmax_{element}$ to the effective water discharge flowing at the silicone-bed interface ($Q_{int}$), which is approximately 25% of the measured water pump discharge (Lelandais, 2018). If $Qmax_{system} < Q_{int}$ we consider the drainage system as inefficient, while if $Qmax_{system} \geq Q_{int}$ we consider the drainage system as efficient. $Q_{max}$ might be overestimated since we are not able to measure the silicone creep that possibly decreases the hydraulic radius of drainage elements.

We define the drainage cover index ($D_{ci}$) (**3**) as the ratio between the area covered by the drainage network and the area covered by the silicone lobe. The lobe area is delimited laterally from the rest of the silicone cap by inflection points at the margins of the protruding lobe (**Fig.1C**). $D_{ci}$ is an adaptation of the drainage density classically used to describe watersheds, landscape dissection, run-off potential and drainage efficiency in subaerial water drainage systems (Yang and others, 2022).

$$(3)\ \mathrm{D}ci = \frac{Surface\ covered\ by\ the\ drainage\ system}{Surface\ covered\ by\ the\ silicon\ lobe}$$

Finally, to compare the extent of silicone lobes between various experiments, we compute the lobe cover index ($L_{ci}$) (**4**) as the ratio between the area covered by the silicone lobe and the total area of the silicone cap.

$$(4)\mathrm{L}ci(\%) = \frac{Surface\ covered\ by\ the\ silicone\ lobe}{Surface\ covered\ by\ the\ silicone\ cap}$$

*2.1.3. Scaling*

Considering that this model uses water and silicone for simulating meltwater and ice respectively, the rules of a classical scaling in which the model is a perfect miniaturization of nature are not practical (Paola and others, 2009). The use of silicone putty also induces a major scaling limitation since the viscosity ratios between the cap materials, either ice or silicone putty, the basal fluid, water in both cases, are different. In this perspective, Lelandais and others (2016) based the scaling of this model on the displacement of the natural ice and experimental silicone margins through time. They used a unit-free speed ratio between the silicone and ice margin velocity and the incision rate of experimental and natural tunnel valleys. In this way, the complexity of the relations among subglacial hydrology, subglacial erosion and ice flow, which is one of the main issues in numerical modeling, is included in the velocity values. The scaling attests that the value of the ratio between margin velocity and incision rate of tunnel valleys in the experiment falls within the field validity defined by the range of natural settings.

***Table 1**. Comparison of water drainage and silicone flow characteristics, respectively for surge-like and stream-like silicone flow regimes.*

| Water drainage characteristics | Surge-like flow regime (n= 17) | Stream-like flow regime (n= 7) |
|---|---|---|
| ***Nature of drainage elements*** | Tunnel valleys with multiple tributaries | Mainly channels with no tributaries |
| ***Distribution of drainage elements*** | Radial distribution, tunnel valleys connected to the margin | Radial distribution, channels often disconnected to the margin |
| ***Dimensions of drainage elements*** | Length average: 7.8 cm (4 cm to 15 cm)<br>Width average: 12 mm (3.5 mm to 30 mm)<br>Depth average: 0.9 mm (0.5 mm to 1.7 mm) | Length average 3.4 cm (1.8 cm to 6 cm)<br>Width average 4 mm (2 mm to 10 mm)<br>Depth average 0.4 mm (0.2 – 0.6 mm) |
| ***Morphological characteristics of drainage elements*** | U-shaped cross profile most common<br>Undulating long profile with overdeepenings and adverse slopes<br>Rectilinear, meandering or anastomosed (rare) tunnel valley system<br>Sinuosity index average: 1.15 (1 to 6) | U-shaped cross-profile most common<br>Undulating long profile with overdeepenings and adverse slopes<br>Rectilinear channels<br>Sinuosity index average: 1 |
| ***Number of drainage elements*** | Average per experiment : 2,6 (1 to 9) | Average per experiment : 8,5 (3 to 17) |
| ***Drainage cover index ($D_{ci}$)*** | 21.8 % (12.7 to 34.2) | 7.5 % (4.6 to 10.2 %) |
| ***Drainage efficicency evolution*** | Becoming efficient (after 10 to 20 minutes) | Keep inefficient throughout experiments |
| ***Drainage type*** | Well-channelised, water flow focuses in tunnel valleys | Poorly-channelised, distributed water flow (water film at the silicon-bed interface) |
| ***Formation of drainage elements*** | Tunnel valleys only formed by regressive erosion | Channels either formed by regressive or downstream erosion |
| ***Silicone flow characteristics*** | | |
| ***Flow velocity evolution*** | Rapid decrease of flow velocity after initial outburst flood, follows drainage efficiency evolution | Very slow decrease of flow velocity after initial outburst flood, follows drainage efficiency evolution |
| ***Final lobe cover index ($L_{ci}$)*** | 9 % (4.2 to 10.1%) | 36 % (20.3 to 54.4%) |
| ***Slicone lobe characteristics*** | Thicker lobe and steeper marginal front | Thinner lobe and smoother marginal front |
| ***Development of shear margins*** | Transitory (during surge) | Sustained |

### *2.1.4. Model limitations*

The model is designed to explore the basic mechanical interactions between a simplified water-routing system, a deformable, permeable and erodible sedimentary bed and an impermeable viscous cover. The formation of drainage landforms in the experiments involves interactions between the silicone putty, the injected water and the sand bed. The silicone putty is Newtonian, isotropic and impermeable. Under the experimental conditions (between 15–20 °C and at atmospheric pressure), its viscosity is nearly independent on temperature and the bed keeps constantly wet and saturated. Consequently, temperature-dependent processes (shear heating, heat softening, melting and freezing) and shear softening/hardening related to the non-Newtonian behavior or the anisotropy of ice are not reproducible. Newtonian silicone putty is also unable to localize viscous deformation when stress increases (in particular along lateral shear margins) or to produce fractures in the range of experimental flow velocities we can simulate. Consequently, spatial velocity gradients are expected to be smaller in the experiment than in nature and the width of experimental lateral shear margins is overestimated compared to the width of experimental ice streams (Vérité and others, 2021). Internal production of meltwater, complex spatial variations in subglacial hydrology, and lobe margin ablation and retreat are not reproducible either. The model, like all models, is not perfectly realistic since it reproduces neither a complete and scaled miniaturization of nature nor all subglacial physical processes.

## 2.2. Progress of experiments

*2.2.1 Onset of fast silicone flow (stage I; Fig. 2)*

In all experiments, as long as no water is injected, the silicone cap is coupled to the bed and spreads under its own weight. The silicone cap displays the typical parabolic surface profile of an ice sheet; it increases in diameter and decreases in thickness with time, thus producing a radial pattern of horizontal velocities.

When water injection starts, all experiments behave similarly: injection of water within the bed triggers the formation of a water pocket at the silicone-bed interface and leads to silicone-bed decoupling. After a few minutes, the water pocket migrates outwards and drains suddenly through a distributed network that feeds an outburst flood at the margin of the silicone cap. In all experiments, the migration of the water pocket is coeval with the formation of a corridor of high silicone flow velocity (from 0.07 to 0.09 $mm.s^{-1}$) referred to as an experimental ice stream in previous studies (Lelandais and others, 2016; 2018; Vérité and others, 2021) (stage I; **Fig. 2**). During the flood, two shear bands characterised by high shear strain rates form on either side of the corridor of water migration (**Fig. 2**).

Depending on the subsequent evolution of the subsilicone drainage type and efficiency, two different silicone flow velocity regimes appear later in the experiments: (1) surge-like flow regime (n=17 experiments), characterised by transitory silicone speed-ups and (2) stream-like flow regime (n=7 experiments), characterised by sustained high silicone flow velocities.

*2.2.2 Surge-like flow regime (stages II to IV; Fig. 2)*

In the first class of experiments (Table 1), the distributed system associated with drainage of the initial water pocket collapses into a channelised system comprised of 1 or 2 drainage elements fed by tributaries at their heads and connected with the silicone margin. These initiate below the margin of the silicone cap and gradually expand upstream, by retrogressive erosion of the bed (Stage II; **Fig. 2**).

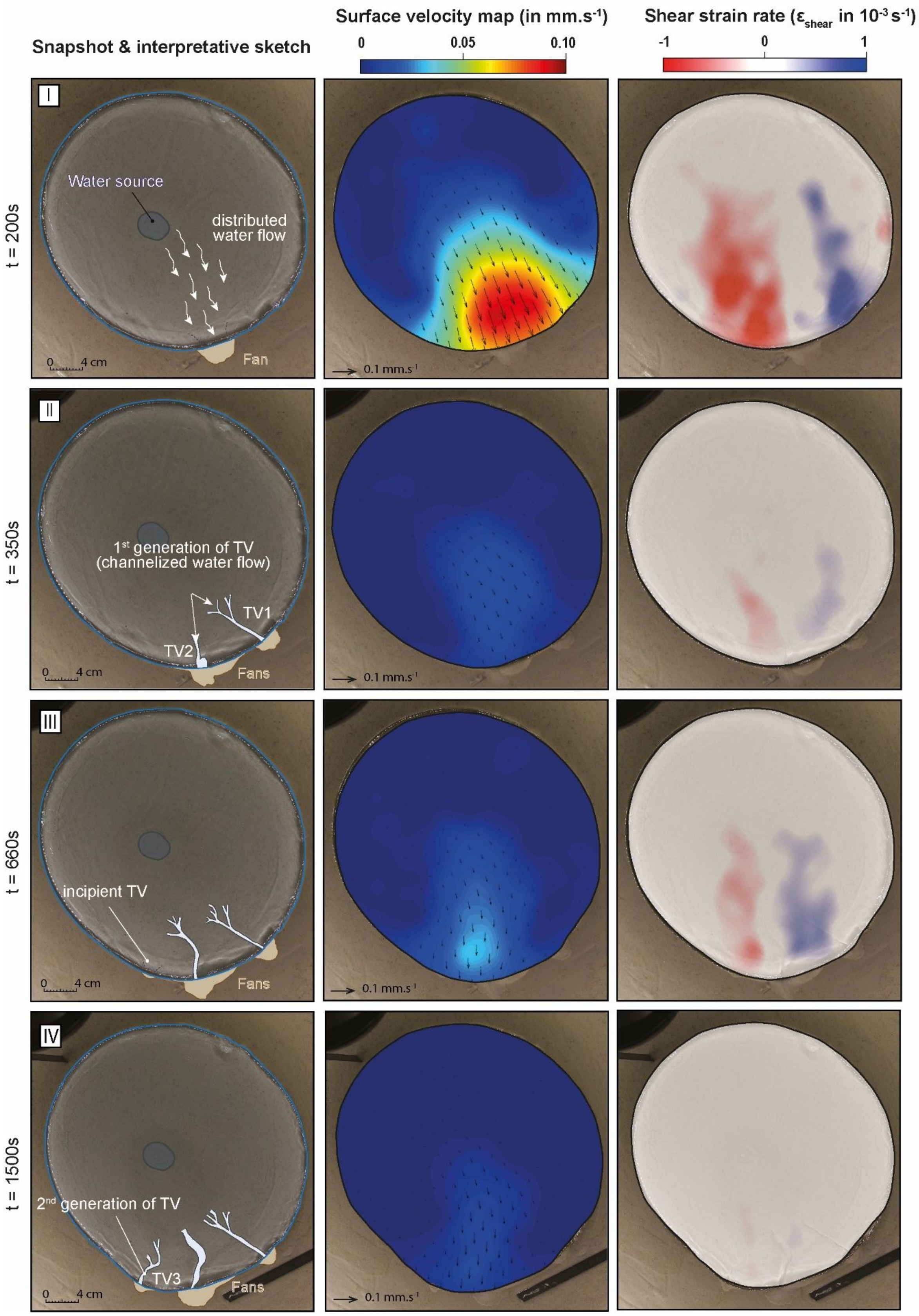


For the experiment shown in Figure 2, the drainage features are respectively 30 and 80 mm long, 12 and 10 mm wide and 0.5 mm deep. For this type of experiments, the drainage features have constant widths along their paths, undulating long profiles, slight sinuosity (1.15 sinuosity index) and a radial distribution (**Table 1**; **Fig. 3A**).

***Figure 2***. *Typical evolution scenario for the first class of experiments (surge-like flow regime) illustrated with interpreted snapshots, surface velocity maps and surface shear strain rate maps.* ***Stage I****: silicone surge and development of shear margins coeval with the drainage of the initial water pocket.* ***Stage II****: silicone slowing during the channelization phase; formation of Tunnel Valleys (TV).* ***Stage III****: Second and minor surge, lateral migration of the fast-flowing silicone corridor and formation of a new tunnel valley.* ***Stage IV****: Silicone flow stabilisation to pre-injection velocity; shear margins vanish while tunnel valleys keep expanding.*

After the initial surge in flow velocity above the draining water pocket, the fast silicone corridor slows down (flow velocity drops to a fourth of the surge speed) and narrows down in response to drainage channelisation (Stage II; **Fig. 2**). The deceleration of silicone is associated with a decrease in shear strain rates along corridor lateral margins. A new transient water pocket grows below the silicone cap, migrates and drains next to the existing valley system to form a new outburst flood (Stage III; **Fig. 2**). This new drainage pathway induces a reacceleration of the silicone flow (15% speedup, sometimes more) and shear bands strengthening. A possible relocation of the corridor of faster flowing silicone is possible if the transient water pocket drains laterally to the existent channelised system. The new outburst flood is generally associated with the initiation of a 2nd generation of drainage features in a hitherto slow-moving region of the silicone cap (Stage III; **Fig. 2**).

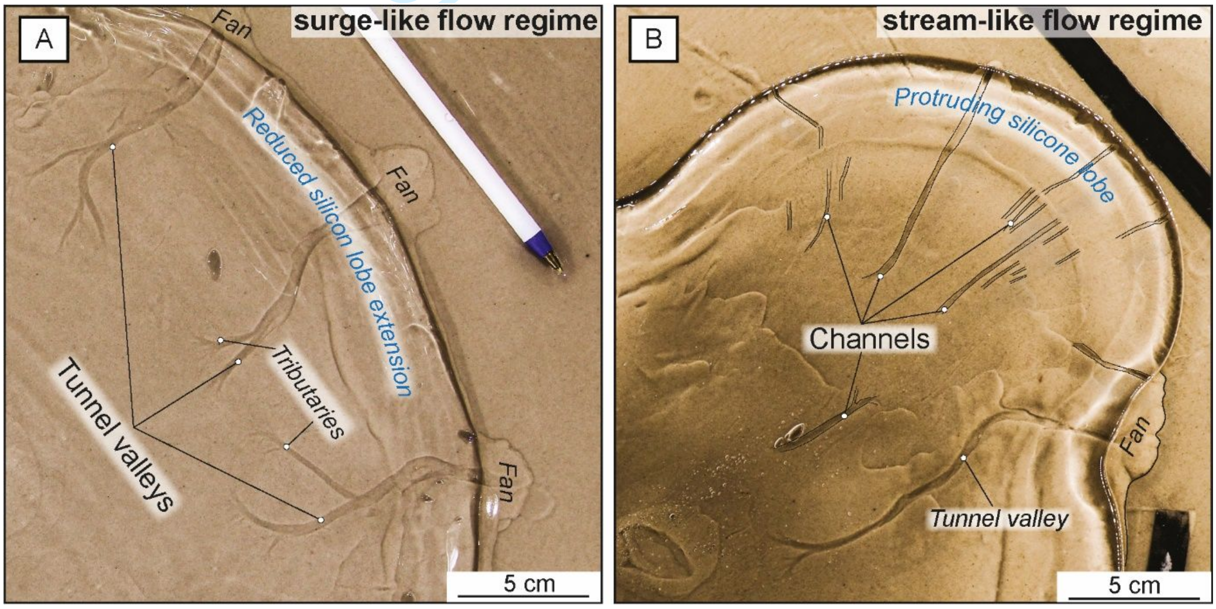


***Figure 3.*** *Snapshots of drainage features reproduced experimentally during surge-like and stream-like flow experiments. (A) Slightly sinuous tunnel valleys with tributaries connected to a silicone lobe margin typical of the surge-like flow regime scenario. (B) Multiple rectilinear channels of smaller dimensions often disconnected from margin and associated with protruding silicone lobe emerging from silicone stream. Note that the tunnel valley in panel B is becoming quickly inactive while channels keep forming.*

The expansion (by regressive erosion and deepening) of existing drainage elements and associated marginal fans continues until the end of the experiment (Stage IV; **Fig. 2**). After 1800 s, the average drainage cover index (D*ci*) is 21.8% (12.7 to 34.2%). Experiments of this kind display 2.6 drainage elements on average (1 to 9) and their final dimensions are 78 mm long, 12 mm wide and 0.9 mm deep on average (**Table 1**). Following expansion of drainage features, the flow velocity quickly decreases, lateral shear bands vanish and the silicone cap gradually recovers a radial flow pattern similar to the pre-injection phase (Stage IV; **Fig. 2**). Focused silicone flow along a corridor fitting the spatial cover of the water drainage route is associated with the formation of reduced silicone lobes displaying an averaged lobe cover index (L*ci*) of 9 % (4.2 to 10.1 %) (**Table 1**; **Fig. 3A**). Thick and steep lobe margins predominate throughout surge-like flow regime experiments.

*2.2.3 Stream-like flow regime (Stages II to IV; Fig. 4)*

In the second class of experiments, distributed drainage of the initial water pocket is followed by channelisation and formation of a drainage element. For the experiment shown in **Figure 4**, this element expands upstream from the margin by regressive erosion to reach its maximal size (12.5 cm long, 11 mm wide and 1.2 mm deep) at about 600 s (stage I). Both the drainage element and its associated marginal fan show no sign of further expansion after 600 s. After 650 s, a new generation of drainage elements appears, composed of several small (10 to 60 mm long, 2 to 6 mm wide, 0.2 to 0.6 mm deep) rectilinear segments often disconnected from the silicone margin, devoid of tributaries, and growing mostly by downstream erosion (stages I and II; **Fig. 4**). This generation is followed by others that contribute to form up to 15 distinct and disconnected drainage elements arranged in a radial pattern below the silicone lobe (stages III and IV; **Fig. 4**). Their dimensions are in average twice to thrice smaller than drainage elements observed for the surge-like class of experiments (**Table 1; Fig. 3B**).

After 30 minutes, the D*ci* for stream-like experiments is 21.8% (12.7 to 34.2%) and the average number of single drainage elements is 8.5 (3 to 17). The velocity of the silicone margin gradually decreases during the experiment (from 0.09 $mm.s^{-1}$ to 0.04 $mm.s^{-1}$) but stabilizes at about 0.04 $mm.s^{-1}$ from 1700 s to the end (**Fig. 4**). Once the water pocket has drained, a corridor of fast silicone flow bordered by two lateral bands of high shear strain rates maintains throughout the experiment. Following the trend of silicone flow velocity, surface shear strain rates slowly decrease before stabilizing at the end of experiments. Focused fast silicone flow is associated with the formation of protruding lobes characterised by an average L*ci* of 36 % (20.3 to 54.4 %) (**Table 1**; **Fig. 3B**). Thinner lobes with smoother margins are observed at the end of stream-like flow regime experiments.

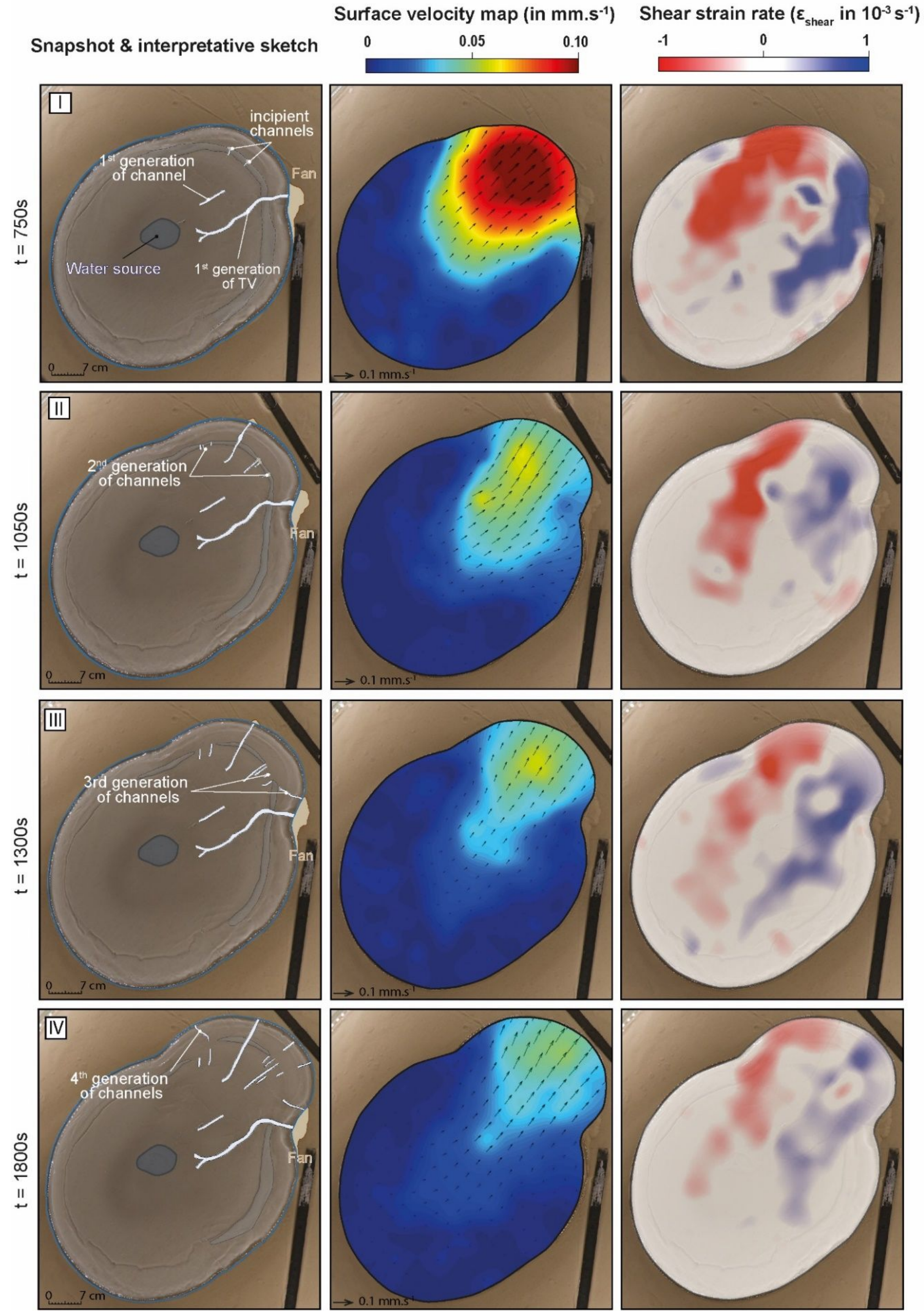


***Figure 4**. Evolution of the second experimental scenario (stream-like flow regime) described with interpreted snapshots, surface velocity maps and shear strain rate maps. **Stage I**: Sustained high silicone flow velocity (triggered during outburst flood, cf. stage I in Fig. 2) although channelization was initiated through formation of a tunnel valley. Minor channels form in parallel due to rapid cessation of the tunnel valley activity. Shear bands delineating the margin of a fast-flowing silicone corridor are observed. **Stages II to IV**: Tunnel valley is inactive, multiple generation of small water channels form, many of them being disconnected from the margin. The magnitude of silicone flow velocity and shear strain rates maintain at high levels throughout the experiment.*

### 2.3. Response of silicone flow dynamics to changes in drainage efficiency

*2.3.1. Surge-like flow regime*

After the first six minutes following the channelisation of water flow, the maximal discharge capacity ($Qmax_{system}$) of the drainage network in the first class of experiments (**Figures 2 and 5A**) has reached a third (0.3 $10^{-6} m^3 s^{-1}$) of the effective water discharge at the silicone-bed interface ($Q_{int}$). $Qmax_{system}$ has thus increased after the initial outburst flood, by initiation and expansion of two drainage elements. This increase in discharge capacity contributes to quickly decrease (from 8 $mm.s^{-1}$ to 2 $mm.s^{-1}$ in 200 s) the silicone flow velocity that almost recovers pre-surge values, although the drainage remains inefficient ($Qmax_{system} < Q_{int}$). From 800 s to 1000 s, the transitory migration and drainage of a secondary water pocket triggers a second and minor surge in silicone flow velocity (**Fig. 5A**). This second surging event starts receding after 150 s with the growth of a new drainage element further increasing the maximal discharge capacity of the whole drainage network. On both sides of the surging corridor, transient shear margins develop during the two silicone speed up phases and quickly fade when silicone decelerates. Considering that all drainage elements are actively draining water, we estimate that $Qmax_{system} > Q_{int}$ after 1100 s (**Fig. 5A**). From this point, the drainage becomes and remains efficient throughout the rest of the experiment, due to continuous expansion of the drainage network. After 1800 s, the value of $Qmax_{system}$ is almost twice that of $Q_{int}$. In response to this increasing drainage efficiency, the silicone flow velocity keeps decreasing and two bands of high shear strain rates almost completely vanish. Efficient drainage and decrease of flow velocity imply that all water drained at the interface is flowing in the channelized drainage system and that friction related to silicone-bed coupling occurs outside the drainage system. A quiescent phase (in between surges) is reached at the end of the experiment when the silicone flow velocity recovers pre-injection flow velocity (**Figs. 2 and 5A**).

*2.3.2. Stream-like flow regime*

After the initial outburst flood, **Figures 4** and **5B** show that channelization can lead to the development of one single drainage element that increases in size to reach a $Qmax_{system}$ of $0.6 \cdot 10^{-6} m^3 s^{-1}$, approximately half the value of $Q_{int}$. This increase in maximal drainage capacity is coeval with a 10% deceleration of the silicone flow. When the drainage element ceases to grow and the water is re-routed toward smaller drainage elements, $Qmax_{system}$ first falls, then increases gradually as new drainage elements form. After 20 minutes, $Qmax_{system}$ has tripled (from 0.2 to 0.6 $10^{-6} m^3 s^{-1}$) but remains lower than $Q_{int}$, implying that inefficient drainage persists throughout the experiment. This implies that part of water flowing at the interface either accumulates upstream, flows outside the channelised system as a thin and distributed water film. Maintained high silicone flow velocities during the entire experiments imply that part of the water flows as a distributed water film lubricating the silicone-bed interface. During the development of the drainage network, the silicone flow velocity decreases with respect to the peak velocity observed during the outburst, but remains more than three times higher than before the outburst, thus allowing the shear bands to maintain (**Fig. 5B**).

### 2.4. Ice surge vs. ice stream: controlled by the evolution of drainage efficiency

#### *2.4.1. Transitory fast ice flow and efficient drainage: surge-like flow regime*

The surge-like regime observed in most experiments (**Figs. 2, 5A**; **Table 1**) is characterised by transient and repeated formation of fast-flowing silicone corridors and rapid reorganization of the hydrological system induced by focused erosion along water passageways that increase the maximum drainage capacity ($Qmax_{system}$). This rapid change of drainage capacity, by increasing the amount of water that can flow within drainage passageways, controls the evolution of drainage efficiency and modulate the surging character of the flow.

In the first stages of these experiments, drainage inefficiency is evidenced by water ponding and subsequent outburst flood fed by an inefficient and distributed drainage related to migration of the transient water body. Drainage inefficiency is associated with silicone flow speed up, incipient lobation of the margin and development of shear margins on both sides of the fast-flowing silicone corridor (**Figs. 2, 5A**). Formation and migration of subglacial water bodies have been mapped or inferred beneath modern and former ice sheets (Fricker and others, 2007; Carter and others, 2017) and associated with ice flow speed-up events (Bell and others, 2007; Stearns and others, 2008; Siegfried and others, 2016). Outburst events are known to promote ice-bed decoupling, basal lubrication and thus ice flow acceleration (Alley and others, 2006; Bell and others, 2007; Magnússon and others, 2007; Stearns and others, 2008; Livingstone and others, 2016; Lelandais and others, 2018). In our experiments, once flooding ceases, the hydrological system reorganises, the distributed drainage collapses into large and fast expanding drainage passageways we interpret to be the experimental counterpart of tunnel valleys considering their morphological similarities (U-shaped cross-sectional profiles, undulating long profiles, constant widths) (Lelandais and others, 2016). Lengths, widths and depths of single tunnel valleys are in average twice to thrice bigger than water passageways observed in streaming experiments. The drainage network is characterised by smaller numbers of drainage elements in average (2.6 vs. 8.5 for streaming) and a subsequent lower Dci (7.5% vs 21.8% for streaming experiments), suggesting that the degree of channelisation controls the evolution of silicone flow velocity. As the drainage efficiency increases, the ice flow quickly decelerates and the shear margins dissipate suggesting that the flow speed up period is short enough to be comparable to glacier surges (Dowdeswell and others, 1991). The transitory nature of the flood and associated speed up event is comparable to glacier surges where the increase of flow velocity is limited in time (from days to years) and generally bounded by quiescent phases where ice flow velocity is much slower. The basic definition of a surge-type glacier includes that major fluctuations in velocities are periodical and not restricted to a single speed up event (Benn and Evans, 2010). In our experiments, other minor and quick surges (**Figs. 2, 5A**), related to the release of successive water pockets strengthens the surge-like behavior of the silicone experiments by showing multiple speed-up events of different magnitudes interspersed with quiescent phases characterised by much slower silicone flow. These successive surges, corresponding to the drainage of new water pockets, fit the observations made by Cowton and others (2013) in which the existing drainage system is inferred to be channelised but channels are regularly overwhelmed by the transient release of meltwater (from either supraglacial or subglacial sources), triggering episodic speed-up events.

The speed-up events of natural glaciers are generally compensated by a slowdown observed at seasonal (Sole and others, 2011) to multi-seasonal (Sund and others, 2014; Sevestre and others, 2018) timescales. Numerical models and observations indeed predict an abrupt termination of surges due to the discharge of water from the bed, either via a high-storage distributed system or a switch to an efficient channelised system (Benn and others, 2019). This is consistent with previous work led on the hydrology of surge-type glaciers that has shown abrupt surge terminations triggered by step changes in drainage efficiency (e.g. Kamb and others, 1985; Kamb, 1987). However, we observe that the end of the surge event in our experiments is not so abrupt but rather gradual as $Qmax_{system}$ gradually increases while the tunnel valley system keeps expanding (**Figs. 2, 5A**). Some surges have indeed shown gradual slowdowns spreading over multiple seasons (e.g. Luckman and others, 2002; Sund and others, 2014; Sevestre and others, 2018; Benn and others, 2019). The increase of $Qmax_{system}$ might be overestimated as we measure the volume of drainage conduits considering they are filled by water at a bankfull stage. We alternatively hypothesize that the ongoing vertical erosion in tunnel valleys is balanced by the silicone creeping inside the valleys once efficiency is reached and water pressure balanced, leading to stable maximum drainage capacity. The achievement of drainage efficiency is responsible for a gradual decrease of basal water pressure and flow velocity until stagnation of the overlying silicone cap and recovering of a radial flow pattern. Between 1985 and 1994 and 2007 and 2014, Tedstone and others (2013, 2015) observed a 12% decrease in mean annual ice velocity across a land-terminating area of the Greenland ice sheet at the same time as melt rates increased by ~ 50%. They argued that the decrease in velocity is likely the result of the seasonal formation of larger and more frequent subglacial channels extending further into the ice sheet and acting as low pressure arteries for meltwater drainage. For longer timespan, relatively stable channelised system was suggested to promote sustained efficiency of subglacial drainage from beneath the British Ice Sheet, potentially slowing or even arresting the advance of the ice sheet in eastern England during the Middle Pleistocene (Phillips and others, 2013).

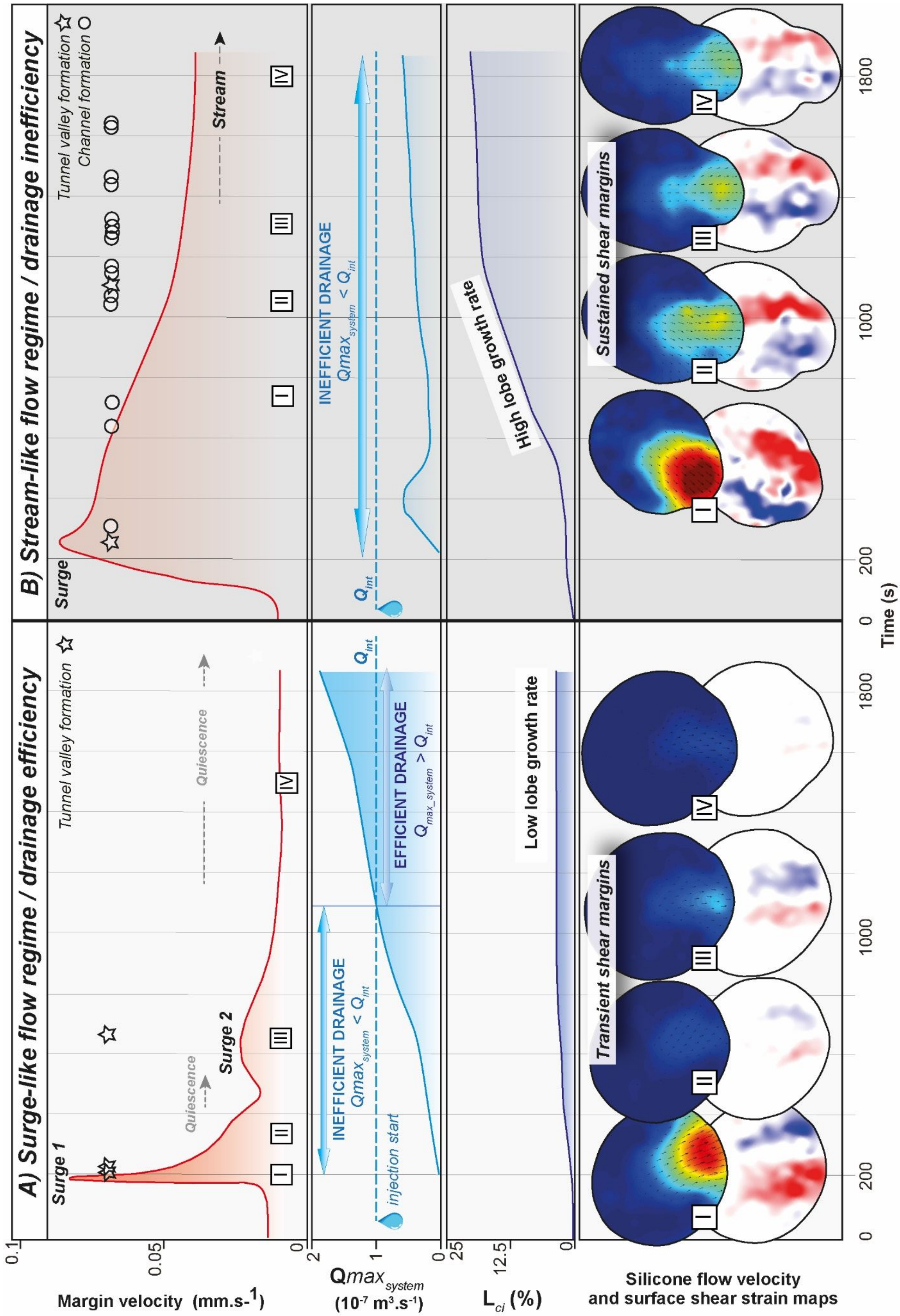


*Figure 5. Monitoring of the evolution of margin velocity (in the axis of the faster flowing zone), drainage capacity of the active valley network ($Qmax_{system}$), silicone lobe cover index ($L_{ci}$), flow velocity and silicone shear strain rate maps respectively for surge-like (A) and stream-like (B) flow regime experiments.*

Experiments show that the sudden release of water (outburst flood) can initiate surging flow while post outburst channelization can be responsible for ice flow quiescence, highlighting the dual response of ice dynamics trough time to the transient release of stored meltwater. Similar surge dynamics has been observed at Kyagar glacier (Karakoram; China) where an abrupt deceleration occurred simultaneously with a lake outburst (Round and others, 2017). They interpreted that opening of subglacial channels during the lake outburst triggered the reduction of subglacial water pressure and, hence, velocity beneath the whole glacier tongue within only 11 days. Our model simulates the so-called hydrologic switch mechanism (from distributed inefficient to channelised efficient), known to be responsible for surge-like glacier dynamics for many outlet glaciers worldwide including Svalbard, Greenland and Alaska (Kamb and others, 1985; Murray and others, 2003; Jiskoot and others, 2003; Jay-Allemand and others, 2011). It is however important not to consider this mechanism as a simple binary switch since both drainage types can exist simultaneously on different parts of the same glacier (Benn and others, 2019), acting as multiple drainage subsystems, with abrupt transition in time and space between each types (Rada and Schoof, 2018).

*2.4.2. Sustained fast ice flow and drainage inefficiency: the stream-like flow regime*

The stream-like regime observed in some experiments (**Figs. 4, 5B; Table 1**) is characterised by sustained high-silicone flow velocity along corridors. The water delivered to the bed is not counterbalanced by sufficient maximal drainage capacity (Q$max_{system}$) leading to an increase of basal water pressure, distributed drainage and higher sliding rates.

Following the initial outburst flood, a silicone surge is triggered as the drainage system is unable to evacuate the input of meltwater from the transient water body migration and drainage (**Figs. 4, 5B**). The drainage system is inefficient, the water drainage is distributed, basal lubrication enhances the silicone flow velocity and shear bands emerge. Channelization occurs after the flood dissipates with the development of one large tunnel valley (**Fig. 4**). The fast expansion of the tunnel valley suddenly stops due to water re-rerouting and tunnel valley abandonment while multiple rectilinear and smaller drainage elements disconnected from the margin start emerging. Based on the morphometric differences, we cannot consider this second type of drainage elements as experimental tunnel valleys and we therefore name them channels. We mainly distinguish tunnel valleys from channels from their dimensions, the occurrence of tributaries and their connectivity to the silicone margin. Another difference is the fact that tunnel valleys are created by the activity of narrow channels which occupy part of them, as river channels occupy parts of valleys. As suggested for some of their natural counterparts (Greenwood and others, 2007; Kehew and others, 2012; Livingstone and others, 2016) channel dimensions are at least half those of tunnel valley (**Table 1**). Their smaller number, dimensions and their inner positions (i.e., disconnected to the margins) confer a lower drainage efficiency to the hydrological network despite the development of multiple channel generations. The inefficiency persists throughout the experiment although $Qmax_{system}$ increases to reach half $Q_{int}$. This initiates a small and very gradual decrease in silicone flow velocity because the drainage inefficiency helps maintaining high sliding rates for a longer timespan (**Fig. 5B**). Compared to the surge-like experimental scenario and referring to previous studies using a similar experimental set up (Lelandais and others, 2018; Vérité and others, 2021), we interpret the silicone flow regime as the experimental counterpart of an ice stream. Generally, ice streaming is used to describe a sustained period of fast-flow (decades to millennia), whereas surge-type glaciers exhibit a cycle of fast-flow (typically years), followed by a quiescent phase that is of much longer duration (typically decades; Raymond, 1987). The stream-like regime, characterised by stabilized high silicone flow velocities, arises from a phase of surge-like flow regime at the beginning of our experiments. This switch in the type of fast-flow regime correlates with the inability of the drainage landsystem to achieve drainage efficiency. Similarly, Zheng and others (2019) have for the first time observed the birth of an ice stream on Vavilov Ice Cap after recording a surge-like behavior for several years (Zheng and others, 2019). Indeed, after the initial surge in 2013, the outlet glacier of Vavilov ice cap kept retaining fast-flow at around 1.8 km/year for 6 years, an unusually long-lasting speed for a glacier, suggesting the outlet entered a phase of stream-like flow regime, thus recording a switch in fast-flow regime. This incipient ice stream was associated with the propagation of shear margins representing one of the most distinctive properties of ice streams. Indeed, ice streams are conditioned by the development of sharply delineated shear margins bounding the transition between slow- and fast-moving ice (Raymond, 1996; Raymond and others, 2001; Schoof, 2004). We show that the sustained silicone flow velocity in our experiments is associated with persistent shear margins through calculation of shear strain rates at the silicone surface (**Fig. 4**). We assume that the sustained and focused silicone flow velocity, combined with the development of shear margins strengthen the comparison with natural ice streams (Bennett, 2003). The sustained delivery of fast-flowing silicone to the margin leads to the formation of extensive lobe stretching far beyond the silicone cap margin, sensing the parallel with the well-developed southern Laurentide ice lobes argued to be the outlets of Pleistocene terrestrial ice streams (Patterson, 1997).

Although the stream mechanism is initiated by outburst flooding, sustained high sliding velocities regime are later controlled only by the inefficiency of the drainage system to accommodate constant water input. Hogan and others (2022) suggest that periodical water release from subglacial lakes beneath ice streams, every few tens to hundreds years, might only temporarily affect ice flow velocities for periods of weeks to month and cannot be considered as a mechanism responsible for long-term streaming. Our modelling results rather suggest that long-lived ice stream is possibly related to the inability of the drainage landsystem to accommodate a long-term and sustained meltwater production.

### 2.5. Controls on fast-flow regimes

Thermo-mechanical instabilities resulting from feedbacks between ice flow, water flow and bed deformation have been suggested to control glacial streaming and surging (Fowler and Johnson, 1996; Payne and Dongelmans, 1997; Hindmarsh 2009; Kyrke-Smith and others, 2014; Lelandais and others, 2018; Benn and others, 2019). By analogy, although thermal processes are not simulated in our experiments, the observed stream-like and surge-like regimes may be understood as physical instabilities resulting from mechanical feedbacks between silicone flow, water flow, bed deformation and development of drainage landforms at the silicone-bed interface. The instability tends to disappear and reappear spontaneously, cyclically and rapidly in the surge-like regime, while it persists over longer timescales in the stream-like regime. This difference is controlled by differences in the development of the subglacial water drainage landsystem. Parameters that may control the development of the drainage landsystem include the water injection scenario, the geometrical and rheological characteristics of the silicone cap and the geometrical, rheological and hydrological characteristics of the bed.

We performed our 24 experiments with constant parameters (**Table S1**): we thus hypothesize that the kind of instability that controls the flow regime in the experiments is mostly sensitive to small unmeasurable parameters: these may include lateral variations in bed slope, roughness, topography, compacity or permeability, or variations in the initial geometry (thickness, margin shape, location of water injector) of the silicone cap. If these conclusions may be extrapolated to natural glaciers, this suggests that the flow regime of terrestrial ice lobes resting of flat beds might be so sensitive to small perturbations, that it may be unpredictable and might even switch erratically.

## 3. PALAEOGLACIOLOGY

We selected two neighboring palaeo-ice lobe landsystems beneath the Laurentide Ice Sheet for their obvious differences in dimensions, drainage network and overall landform signature to bridge the gap between experimental results and natural data. This palaeoglaciological approach will contribute to conceptualize relations between subglacial hydrology, ice flow regimes and landform signature based on their visible similarities with experimental results.

### 3.1. Study area

During the Late Wisconsinan glaciation, the Laurentide Ice Sheet (LIS) covered Canada entirely and reached its maximum extent ~21 cal. ka BP (Dyke and others, 2003; Margold and others, 2015) (**Fig. 6A**). Palaeoglaciological reconstructions revealed a relatively stable ice margin of the LIS in north-west mainland Canada until ~16.2 cal. ka BP (Margold and others, 2018). Following this stagnation phase, an ice-free corridor progressively formed along the eastern foot of the Cordilleran Ice Sheet around 14.25 cal. ka BP, after which LIS rapidly retreated eastward until western Canada became ice free around 11.5 cal. ka BP (Dyke and others, 2003). Numerous climate-sensitive ice stream and lobe systems spreading westward thus developed over the Interior Plains, associated with major proglacial lakes (Lemmen and others, 1994; Dyke, 2004).

The study area is located along the palaeo-Great Slave Lake Ice Stream (GSLIS) between the Horn Plateau and Cameron hills (**Fig. 6B**), where several flow sets of lineations illustrate multiple ice flow directions, probably contemporaneous to the ice-streaming phase of the GSLIS. The timing of operation of this ice stream has been calibrated by $^{14}C$ dating and is thought to span between 13.5 and 10.8 cal. ka BP although the exact timing of operation is very uncertain because the whole region has extremely bad data coverage (Dyke and others, 2003; Margold and others, 2018). Moraine complexes associated with drainage features (meltwater channels and tunnel valleys) reveal former lobe positions (Brown and others, 2011), possibly representing the position of GSLIS outlets during deglaciation. We focus on two ice lobes we refer to as the Liard Moraine Ice lobe (13-12.7 cal. ka BP) and the Trout Lake Ice lobe (13 cal. ka BP) (Lemmen and others, 1994; Smith, 1994; Dyke, 2004) (**Fig. 6B**). The LIS entirely retreated from the study area depicted in **Figure 6B** after 12.7 cal. ka BP, to make way for the McConnell Glacial Lake (Smith, 1994).

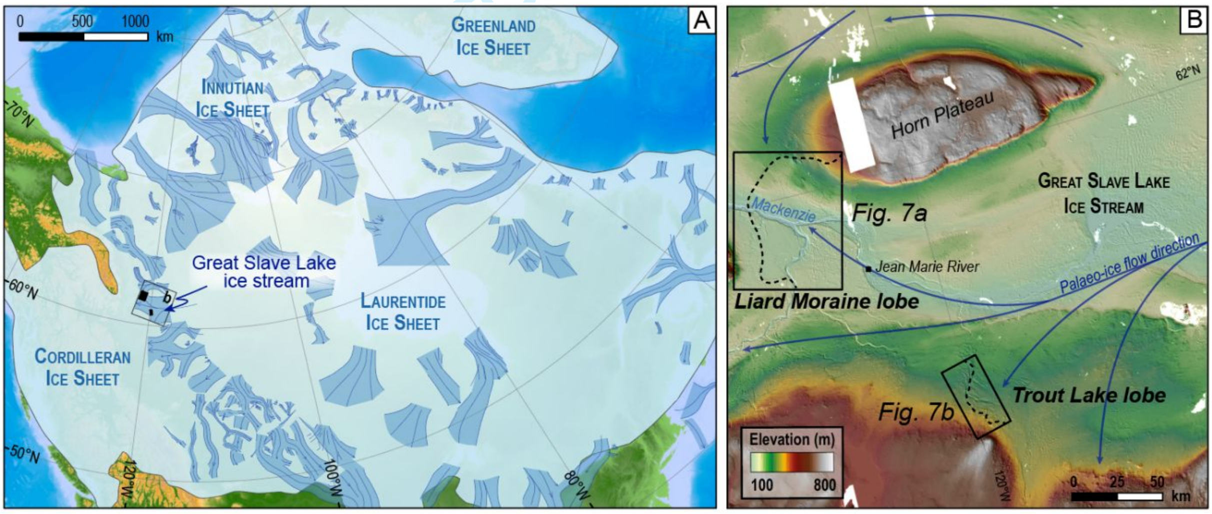


*__Figure 6.__ Geographical and palaeoglaciological context of the study area. (A) Location of the study area in the frame of the Laurentide ice sheet extent during the Last Glacial Maximum and palaeo-ice stream tracks and main flow directions (modified from Margold and others, 2018). (B) DEM of the former Great Slave Lake Ice Stream with black rectangles referring to the two palaeo-ice lobes that have been analysed in details. Dotted curved lines corresponding to former lobe position reconstructed from large end moraine complexes.*

### 3.2. Methods

To identify, map and characterize the drainage network relative to these lobes, we mapped meltwater channels, tunnel valleys and major moraine complexes using a 10-m digital elevation model (DEM) computed by optical stereo imagery (https://www.pgc.umn.edu/data/arcticdem). Using hillshaded DEMs, we digitized drainage networks, marginal and subglacial landforms at the scale of 1:20 000 in a Geographic Information System. The width and depth of drainage features were extracted using regularly-spaced transverse cross sections. The sinuosity index of drainage features was calculated using their channel-parallel length and their straight line length using a “Minimum Bounding

Geometry" tool. The maximum lobe extension area at a given time is roughly approached from the inflection points related to the protruding lobe delimited by major arcuate moraine complexes and the drainage cover index is measured using equation (2).

**3.3. Palaeoglaciological mapping**

*3.3.1. Landform signature of palaeo-ice lobe positions*

*Trout Lake area*

In the Trout Lake area (**Fig. 7A**), a set of 30 patches of moraine ridges, typically 500 m wide, few tens of kilometers long and up to 20 m high, form a nearly continuous and curvilinear morainic complex that draws the position of a palaeo-ice lobe margin. A maximum extension area of 170 $km^2$ is estimated for the Trout Lake Lobe.

*Liard Moraine area*

Ice-marginal landforms are common in the Liard Moraine area (**Fig.7B**). Multiple discontinuous curvilinear and arcuate ridges are observed, indicating former lobe positions. Building upon the work of Brown and others (2011), we have mapped 104 fragments of moraine ridges in the area: they are typically 0.5-1 km wide, up to few tens of kilometers long and 10-20 m high with frequently eroded crestlines. The approximate maximal extent of the ice lobe in the study area can be reconstructed from interpolated junctions between discontinuous major ridges: these form an arcuate moraine complex one hundred kilometers long. A maximum lobe extension area of roughly 1800 $km^2$ can be estimated.

*3.3.2. Palaeo-drainage characteristics*

*Trout Lake area*

In the Trout Lake lobe area, mapped drainage features are erosional only (no eskers). A network of 6 major erosive drainage elements (6-15 km long, 200-700 m wide and 5-25 m deep) characterised by numerous tributaries (1-3 km long, 100-200 m wide and 3-13 m deep) forms a well-developed system of slightly sinuous to braided (mean sinuosity index: 1.09) water passageways (**Figs. 7A; 8A; Table 2**). This network exhibits a clear radial pattern relative to the belt of end moraine ridges indicating the palaeo-lobe margin. Drainage element terminations delineating the palaeo-lobe margin suggest they were active during the ice lobe formation. Drainage elements display variations in widths and depths along their long profiles, U-shaped cross profiles and clear connections with the palaeo-lobe margin. The drainage cover index ($D_{ci}$) measured for this drainage network is 34% (**Table 2**).

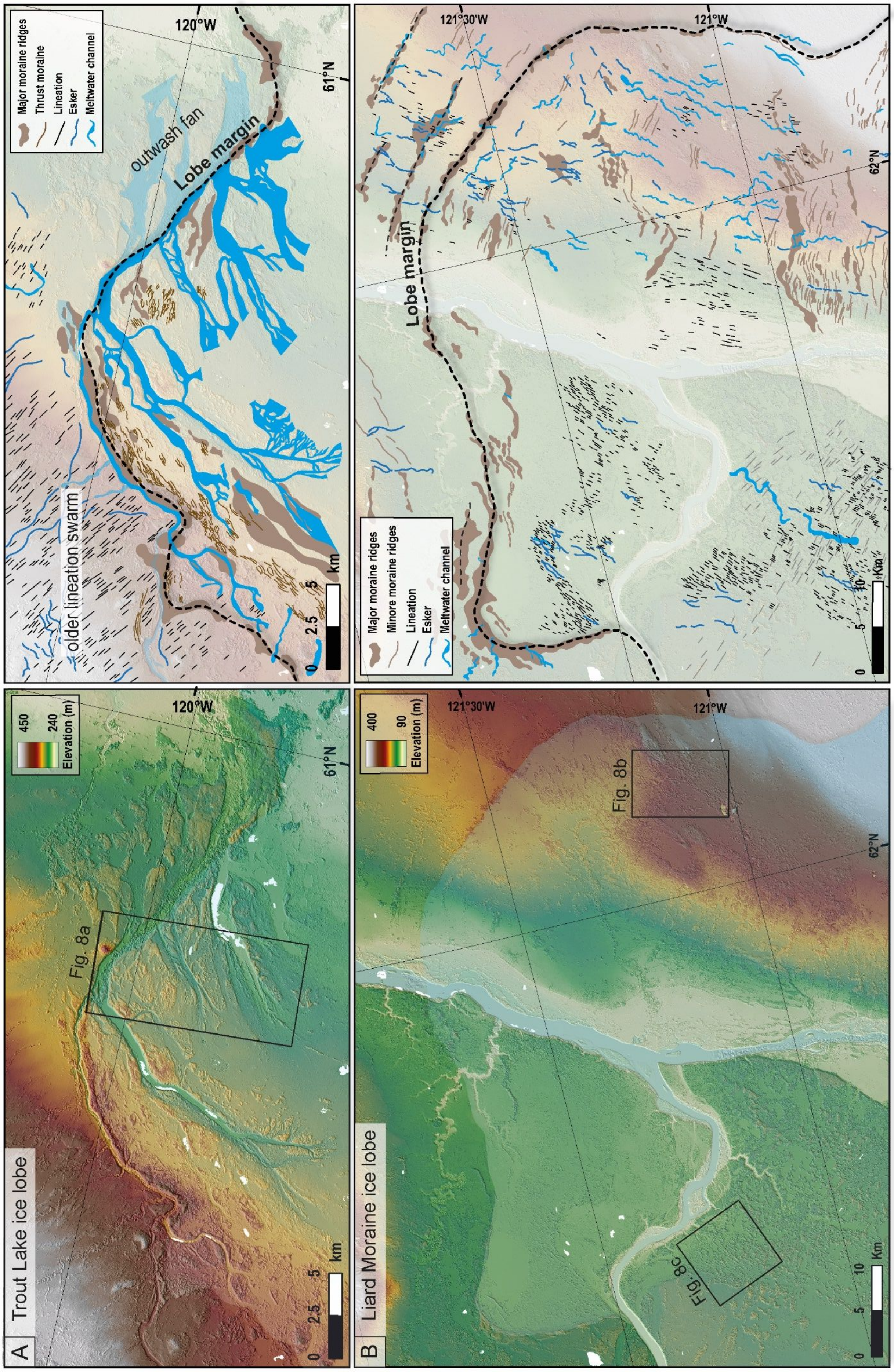


***Figure 7**. DEM and interpreted maps with digitized landforms of the palaeo-Trout Lake (A) and Liard moraine (B) ice lobes.*

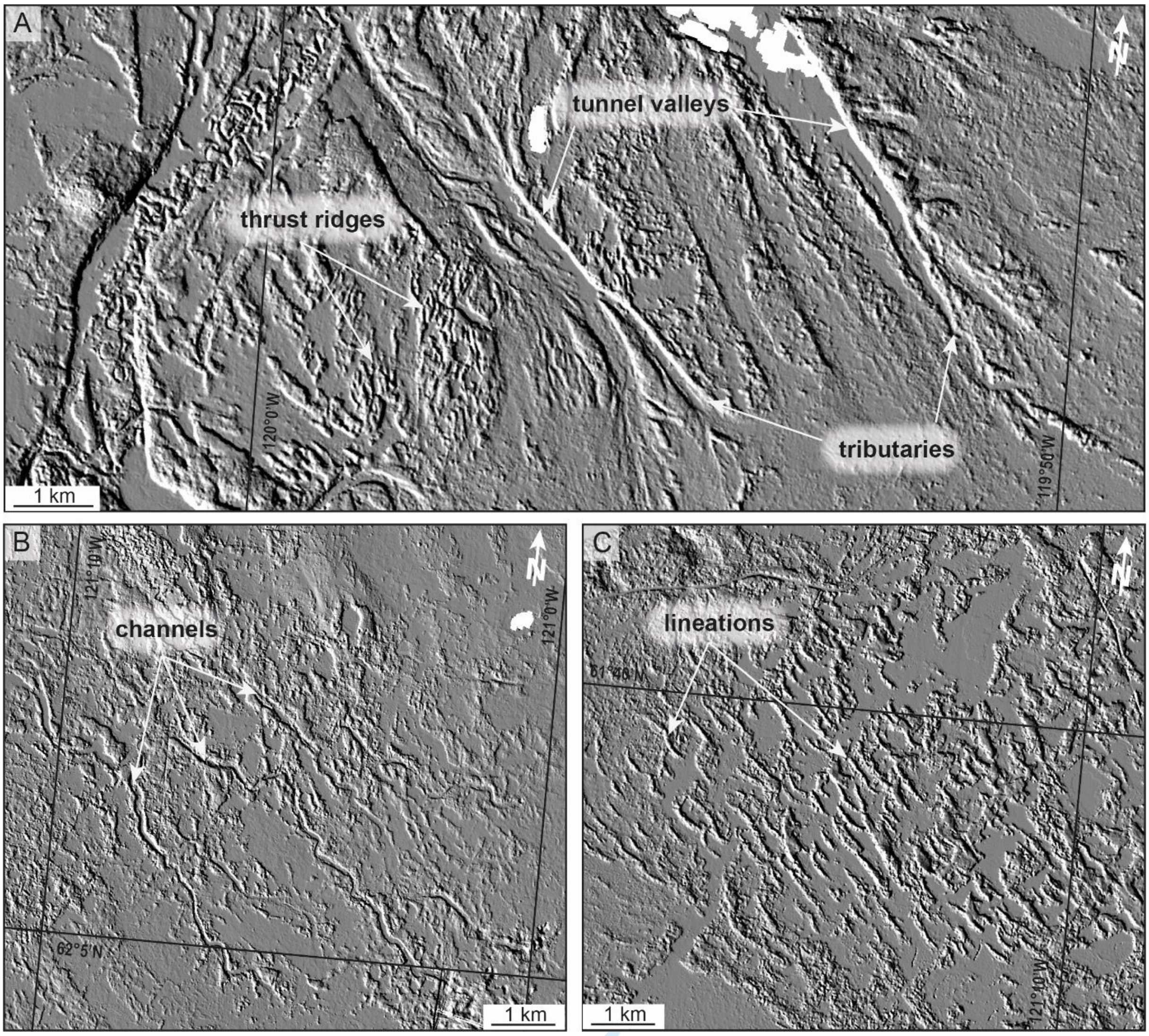


*Figure 8*. *Shaded relief illustrating the drainage features and landform assemblages characterizing the bed of each palaeo-ice lobe mapped in Figure 7. (A) Large tunnel valleys with tributaries observed beneath the Trout Lake lobe. Note the occurrence of closely-spaced ridges interpreted as subglacial thrust ridges in between tunnel valleys. (B) Slightly sinuous and minor channels typically covering the bed of the Liard moraine ice lobe. (C) Lineations swarm taken from the Liard moraine ice lobe.*

### *Liard Moraine area*

Small-scale erosional and depositional features related to meltwater drainage occur in the Liard Moraine Lobe area. We identified 85 single drainage elements: they are 1 to 5 km long and 4 to 12 m deep on average, with constant widths along their paths (110 to 175 m wide). They are rectilinear to slightly sinuous (mean sinuosity index: 1.18) with nearly flat long profiles and are devoid of tributaries (**Figs. 7B, 8B**). A U-shaped cross profile is commonly observed for these water passageways. We also mapped 142 eskers: they display lengths (0.5-2.5 km) similar or slightly lower than channels (**Table 2**). Both erosional and depositional drainage features are concentrated in the area delimited by the belt of major moraine ridges (**Fig. 7B**). They are transverse to the main moraine belt and radially distributed. These drainage features are poorly-connected to each other and commonly disconnected from the inferred maximum lobe margin. Considering the estimation of maximum lobe extension and the hypothesis that the mapped drainage features are contemporaneous to the lobe activity, we compute a drainage cover index ($D_{ci}$) of 2% for the Liard Moraine Lobe.

### *3.3.3. Landform assemblages*

*Trout Lake area*

Upstream from the end moraine delineating the Trout Lake lobe margin, series of closely- and regularly-spaced, parallel or sub-parallel ridges are observed (**Figs. 7A, 8A**). These ridges are often sinuous. They are much smaller in dimensions than end moraines ridges in the area (30-50 m wide, 250-700 long and 3-5 m high). They gather in arcuate belts, 1-2 km in width, that occur parallel to and up-ice from the major end moraine ridges. Considering their pattern and dimension, we interpret those ridges as thrust moraines representing the surface expressions of folds and/or thrust slices formed by subglacial glacitectonism.

**Table 2.** *Comparison of subglacial meltwater drainage and palaeo-ice lobe characteristics, respectively for the Liard Moraine and Trout Lake ice lobes.*

| Meltwater drainage characteristics | Liard Moraine ice lobe | Trout Lake ice lobe |
|---|---|---|
| ***Nature of drainage elements*** | channels with no tributaries and eskers, often disconnected to the ice lobe margin | Tunnel valley with multiple tributaries connected to the ice lobe margin |
| ***Distribution of drainage elements*** | Chaotic distribution of rectilinear to meandering channels | Clear radial distribution of rectilinear, meandering or braided tunnel valleys |
| ***Number of drainage elements*** | Channels: 85<br>Eskers: 142 | Tunnel valleys: 6 |
| ***Dimensions of drainage elements*** | **Channels:**<br>length average : 2942 m (± 1845m)<br>width average : 141 m (± 34m)<br>depth average : 8 m (± 4m)<br>**Eskers:**<br>length average : 1317 m (± 987m) | **Tunnel valleys:**<br>length average : 10166 m (± 4439m)<br>width average : 446 m (± 237m)<br>depth average : 16 m (± 10m) |
| ***Morphological characteristics of drainage elements*** | Constant width and depth<br>U-shaped (& less frequent V-shaped)<br>Flat longitudinal profile<br>Sinuosity index : 1,18 (±0,17) | Fluctuating width and depth of tunnel valleys<br>U-shaped<br>Flat longitudinal profile<br>Sinuosity index : 1,09 (±0,06) |
| ***Drainage cover index (Dci)*** | 2% | 34% |
| ***Drainage type*** | Well-channelised | Poorly-channelised |
| **Palaeo-ice lobe characteristics** | | |
| ***Ice lobe characteristics*** | Large and widespread<br>Partially constrained by topography | Small and localized<br>No topographic control |
| ***Maximum lobe dimensions ($km^2$)*** | ~ 1 800 km2 | ~ 170 km2 |
| ***Associated landforms*** | Arcuate end moraine ridges<br>Lineations | Arcuate end moraine ridges<br>Submarginal thrust masses |

*Liard Moraine area*

Several patches of small-scale lineations, typically 250-600 m long, 50-100 m wide and less than 5 m high, are visible upstream from the lobe margin. They are predominantly transverse to the end moraine belts and do not exhibit overprinting or cross-cutting relationships with other landforms (**Figs. 7B, 8C**), which suggests a synchronous formation with the Liard Moraine Lobe activity. In the periphery of major end moraine ridges, we mapped 208 minor moraines, which form curved belts: they are typically 50 m wide, 0.5-2 km long and less than 5 m high. Following Smith (1994), we interpret them as recessional moraines, formed during the overall lobe retreat, when processes of bulldozing were limited but sediments trapped within ice were yearly deposited by ablation into fine ridges at lobe margin (Chandler and others, 2016).

### 3.4. A landsystem model of drainage efficiency

The efficiency of subglacial drainage is known to control subglacial bed deformation, erosion and glacier dynamics (Benediktsson and others, 2009; Phillips and others, 2013; Lewington and others, 2020), thus the shaping of subglacial landscapes and their constitutive subglacial landform and bedform assemblages (Mäkinen and others, 2017; Vérité and others, 2021, 2022; Dewald and others, 2022). In the light of our experimental and mapping results, we intend to establish the relation between the morphological expression of drainage efficiency and ice flow dynamics to refine landsystem models of either surging or streaming ice lobes (**Fig. 9**).

#### *3.4.1 Efficient drainage signature*

The small Trout Lake Ice lobe (~170 km²) is associated with a well-developed channelised drainage system ($D_{ci}$> 30%) composed of radially distributed drainage passageways that are connected to the palaeo-lobe margin. Their dimensions (2 to 3 times bigger in length, width and depth than channels), connections to the margin, their tributaries and their shapes allow these drainage elements to be considered as tunnel valleys (Kehew and others, 2012; Atkinson and others, 2013).

Tunnel valleys are believed to have been efficient meltwater passageways, lowering the subglacial water-pressure and triggering coupling in between tunnel valleys. Ice-bed coupling in between tunnel valleys is recorded through the development of a submarginal belt of thrust-block moraines paralleling the lobe margin, only locally interrupted by the course of tunnel valleys (**Figs. 7A, 9A**). This is consistent with interpretations, derived from the identification of a subglacial drainage network beneath Humboldt glacier (northern Greenland), that focused water drainage causes sticky inter-channel ridges with higher basal friction (Livingstone and others, 2017). We therefore suggest that the submarginal belt of thrust moraines could be typical landform signatures of efficient drainage, widespread ice-bed coupling and compressive stress transmitted to the bed during the post-surge slowdown of ice flow (**Fig. 9A**). Vérité and others (2021) have interpreted some submarginal bedforms distributed in between channelised system in response to ice-bed coupling and high basal shear stress induced by strong down-ice velocity gradients. Due to their regular wavelengths, they interpreted these structures as ribbed bedforms and invoke a process of formation governed by subglacial deformation and development of thrust-like planes in the sedimentary bed. Similarly, Benediktsson and others (2009) proposed that submarginal end moraines can form by thrusting and shearing of glacial deposits at the end of the surging phase of Brúarjökull, especially in zones of efficient subglacial drainage. The submarginal increase in basal friction limits the growth and spreading of the lobate margin of the Trout

Lake ice lobe (Lci thrice lower than the Liard Moraine Ice lobe), emphasized by a rather short and slightly arcuate end moraine ridge.

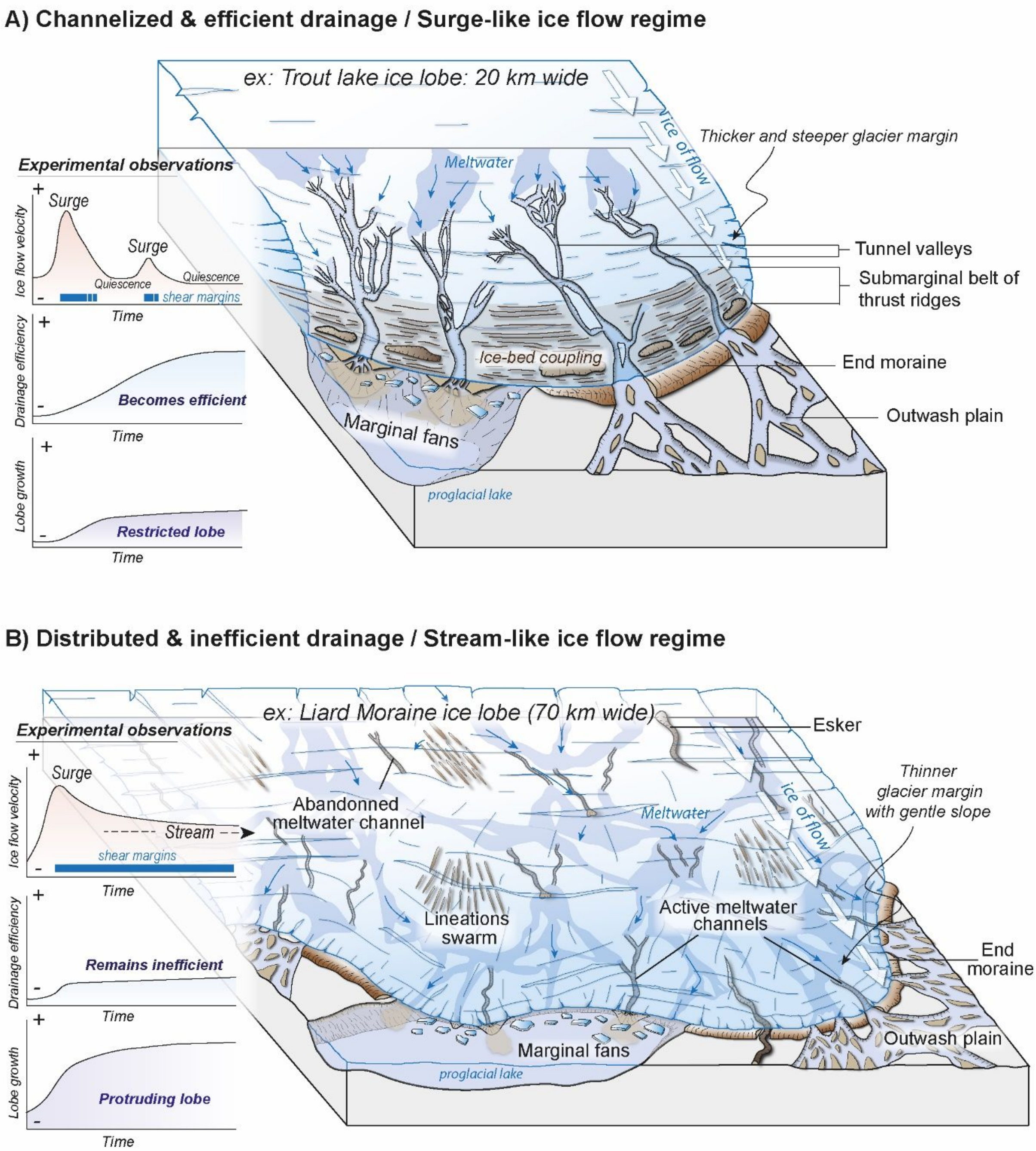


***Figure 9****. Idealised landsystem of channelised efficient drainage (A) and distributed inefficient drainage (B) conceptualised from experimental modelling and palaeoglaciological mapping of two ice lobes of the Great Slave Lake ice stream. The landform signature of each drainage type and ice flow regime is associated with the theoretical evolution trend of ice flow velocity, drainage efficiency and lobe spreading extrapolated from modelling results.*

The absence of lineations beneath the lobe suggests probable lower rate of subglacial bed deformation, either related to lower ice flow velocity or short-lived episodes of high flow velocities (e.g. surges). Seasonal or multi-seasonal increases of subglacial meltwater flow are possible and could temporarily overwhelm the existing drainage network (e.g., spring events), but modelling results and the absence of landforms related to sustained high flow velocity suggest that the drainage network might quickly accommodate transient changes in meltwater discharge. Based on lobe dimensions and characteristics of landform assemblages, and by comparison with experimental results (section 2), we interpret the bed of the palaeo-Trout lake lobe as a landscape relict recording efficient drainage, possibly associated with surging episodes (**Fig. 9A**).

*3.4.2. Inefficient drainage signature*

The Liard Moraine ice lobe is extensive (~1800 km²) and characterised by a poorly-developed drainage system ($D_{ci}$ < 2%), mainly composed of rectilinear drainage elements devoid of tributaries. They are two to three times smaller than the tunnel valleys depicted beneath the Trout Lake ice lobe. Many drainage elements are totally disconnected from the palaeo-ice lobe margin, although some of them are probably not contemporaneous with the maximum lobe extent (**Fig. 7B**). Based on the differences in dimensions, spatial distribution and morphology, we consider that the subglacial drainage system of the Liard Moraine ice lobe is constituted by meltwater channels rather than tunnel valleys (Kehew and others, 2012; Atkinson and others, 2013).

The Liard moraine ice lobe is ten times more widespread than the southern Trout Lake lobe, probably in response to a more sustained input of ice and/or higher ice flow velocities. Multiple swarms of glacial lineations are visible beneath the lobe, indicating either subglacial deformation by fast-flowing ice (Stokes and others, 2013) or subglacial bed deformation over prolonged periods of time (Boyce and Eyles, 1991) (**Fig. 8C**). Sustained ice flow at the outlet of ice streams is suspected to form pronounced and protruding lobate margins when the ice flux is not constrained by topography, evidenced by a long moraine belt (**Fig. 9B**). Patterson (1997) argued that well-developed lobes at the margin of the southeastern Laurentide Ice Sheet represent outlets of terrestrial ice streams analogous in size to those in West Antarctica, suggesting that an ice flux similar to that from Ice Stream B (30 km$^3$ a$^{-1}$: Bindschadler *and others*, 1987) could have created the Des Moines lobe in around 1000 years. Our modelling and the mapping of landforms conducted by Jennings (2006) in Minnesota led to similar conclusions on the conceptualization of connections between ice stream and ice lobe dynamics. To advance beyond the ice sheet, an ice lobe must receive a continuous flow of ice from the ice stream and must therefore sustain high basal water pressure to lubricate the interface. This is made possible by small and rectilinear channels devoid of tributaries enhancing sustained high basal water pressure and sliding rates in response to drainage inefficiency maintained over prolonged periods of time. Based on lobe dimensions, morphology, drainage characteristics and by comparison with experimental results we interpret the bed of the palaeo-Liard moraine ice lobe as a landform relict of an ancient inefficient drainage beneath an outlet glacier fed by an active ice stream (Great Slave Lake Ice Stream) ( **Fig. 9B**).

*3.4.3. Comparison with existing landsystem models*

We suggest that changes in drainage efficiency control fast ice flow regimes (surging vs. streaming) and produce distinct landsystems (**Fig. 9**). We aim to compare our findings to existing landsystem models proposed for ice streams and ice surges. Surge-type and stream-type glacial landsystems share many characteristics that lead some authors to suggest to use modern surge-type glaciers as analogues for ice streams (Ingólfsson and others, 2016), although it is still challenging to figure out if present-day surging processes and landsystem models can be scaled-up and applied to Pleistocene ice streams.

*Surging glacier landsystem*

Bbased upon a combination of observations from contemporary and ancient surging-glacier margins (Evans and Rea, 1999; Benediktsson and others, 2015; Ingólfsson and others, 2016; Evans and others, 2020), classical landsystem models of surging glacier are typically composed of : thrust-block moraines in marginal to submarginal environments, hummocky moraines related to supraglacial melt-out and flowage of debris from stagnant ice, flutes, widespread geometric and sinuous ridge networks (i.e., crevasse and hydrofracture infills) and concertina eskers related to subglacial deformation during the active phase of the surge (Evans and Rea, 1999; Evans and others, 2016; Evans and others, 2022). Most of these typical landforms are neither reproduced experimentally nor observed between the Trout lake lobe. The slow duration of fast-flow events might explain the absence of flutes beneath the Trout Lake ice lobe. Based on our experiments and observations, we suggest that surging is also possibly evidenced by well-developed and channelised tunnel valley systems, characterised by multiple tributaries. Submarginal belt of thrust block moraines in between tunnel valleys must indicate an increase of subglacial bed deformation during surging episodes (**Fig. 9A**).

*Ice stream landsystem*

Most classical ice stream landsystem models are characterised by a corridor of highly elongated glacial lineations (MSGLs), which were postulated to reflect rapid ice velocities (Clark, 1993) bounded by lateral shear margin moraines (Dyke and Morris, 1988; Stokes and Clark, 2002) or ribbed moraine corridors (Vérité and others, 2021). Taken together, these were argued to represent key 'geomorphological criteria' for identifying palaeo-ice streams (Evans and others, 2014; Stokes and others, 2018). The signature of terrestrial-terminating ice streams also encompasses major end moraines ridges, hummocky moraine arcs and possible corridors of geometric and sinuous ridges (crevasse and hydrofracture infills) during the late-stage ice stream activity (Evans and Rea, 1999; Evans and others, 2016; Evans and others, 2022). Lineation swarms, related to sustained fast ice flow, are observed beneath the Liard Moraine ice lobe and are therefore consistent with the classical ice stream landsystem. However, classical ice stream landsystems do not refer to the morphological characteristics of the subglacial drainage network, possibly because both channelised and distributed drainage have been observed beneath modern and ancient ice streams, with possible seasonal or decadal switches from one to another (Davison and others, 2020). We demonstrate a potential morphological signature of prolonged inefficient drainage which is in turn responsible for sustained high ice flow velocity and ice streaming. We suggest that poorly-connected drainage with many small and rectilinear meltwater channels, devoid of tributaries, and often disconnected from lobe margins, could be implemented to existing model, especially for deciphering the contribution of subglacial hydrology to ice stream mechanics (**Fig. 9B**).

## 4. CONCLUSIONS

Experimental modelling and palaeoglaciology contributed to quantify and conceptualise the relations between evolution in efficiency of subglacial drainage landystems and fast ice flow regimes for timescales stretching beyond the available observational record. These approaches especially gave new insights into landsystem models associated with evolution of drainage efficiency and their relations with the duration of fast ice flow events. Rapid increase of drainage efficiency through tunnel valley development that are connected to ice lobe margins reduces the duration of ice flow speed-up events (e.g., ice surges), by decreasing water pressure and promoting widespread coupling. Tunnel valleys, with multiple tributaries, subglacial to submarginal thrust moraines and reduced ice lobe extensions are the most distinctive characteristics of efficient drainage for terrestrial outlets. When tunnel valleys are replaced by rectilinear meltwater channels of much smaller dimensions, the inability of the drainage system to accommodate meltwater input leads to sustained high ice flow velocity (e.g., ice streams). Smaller, disconnected and rectilinear channels, lineations swarms and extensive ice lobes are thought to indicate sustained drainage inefficiency.

These fast ice flow dynamics induced by diverging evolutions in efficiency of drainage landsystems are important to understand the dynamics of terrestrial outlets during deglaciation, especially since the spatio-temporal variations and magnitude of water delivery to the bed remains unknown. Our observations merit repeating and emphasizing because response of land-based outlet glaciers to climate change has been under-explored thus far, compared to their marine counterparts.

**Acknowledgements**

This study is part of the Ice-Collapse project (The dynamics of ice sheet collapse in deglaciation periods) funded by the French Agence Nationale de la Recherche through grant ANR-18-CEO1-0009. It has benefited from the DEFORm projet (Deformation and Erosion by Fluid Overpressure) funded by "Région Pays de la Loire".

## References

Alley, R. B., Dupont, T., Parizek, B., Anandakrishnan, S., Lawson, D. E., Larson, G., & Evenson, E. (2006). Outburst flooding and the initiation of ice-stream surges in response to climatic cooling: A hypothesis. *Geomorphology, 75*(1-2), 76-89.

Ahokangas, E., Ojala, A. E., Tuunainen, A., Valkama, M., Palmu, J.-P., Kajuutti, K., & Mäkinen, J. (2021). The distribution of glacial meltwater routes and associated murtoo fields in Finland. *Geomorphology, 389*, 107854.

Andrews, L. C., Catania, G. A., Hoffman, M. J., Gulley, J. D., Lüthi, M. P., Ryser, C., . . . Neumann, T. A. (2014). Direct observations of evolving subglacial drainage beneath the Greenland Ice Sheet. *Nature, 514*(7520), 80-83.

Atkinson, N., Andriashek, L., & Slattery, S. (2013). Morphological analysis and evolution of buried tunnel valleys in northeast Alberta, Canada. *Quaternary Science Reviews, 65*, 53-72.

Bartholomew, I., Nienow, P., Sole, A., Mair, D., Cowton, T., & King, M. A. (2012). Short-term variability in Greenland ice sheet motion forced by time-varying meltwater drainage: Implications for the relationship between subglacial drainage system behavior and ice velocity. *Journal of Geophysical Research: Earth Surface, 117*(F3).

Bell, R. E. (2008). The role of subglacial water in ice-sheet mass balance. *Nature Geoscience, 1*(5), 297-304.

Bell, R. E., Studinger, M., Shuman, C. A., Fahnestock, M. A., & Joughin, I. (2007). Large subglacial lakes in East Antarctica at the onset of fast-flowing ice streams. *Nature, 445*(7130), 904-907.

Benediktsson, Í. Ö., Ingolfsson, O., Schomacker, A., & Kjaer, K. H. (2009). Formation of submarginal and proglacial end moraines: implications of ice-flow mechanism during the 1963–64 surge of Brúarjökull, Iceland. *Boreas, 38*(3), 440-457.

Benediktsson, Í. Ö., Schomacker, A., Johnson, M. D., Geiger, A. J., Ingólfsson, Ó., & Guðmundsdóttir, E. R. (2015). Architecture and structural evolution of an early Little Ice Age terminal moraine at the surge-type glacier Múlajökull, Iceland. *Journal of Geophysical Research: Earth Surface, 120*(9), 1895-1910.

Benn, D., & Evans, D. J. (2014). Glaciers and glaciation.

Benn, D., Fowler, A. C., Hewitt, I., & Sevestre, H. (2019). A general theory of glacier surges. *Journal of Glaciology, 65*(253), 701-716.

Bennett, M. R. (2003). Ice streams as the arteries of an ice sheet: their mechanics, stability and significance. *Earth-Science Reviews, 61*(3-4), 309-339.

Bindschadler, R. (1983). The importance of pressurized subglacial water in separation and sliding at the glacier bed. *Journal of Glaciology, 29*(101), 3-19.

Bindschadler, R., Stephenson, S., MacAyeal, D., & Shabtaie, S. (1987). Ice dynamics at the mouth of Ice Stream B, Antarctica. *Journal of Geophysical Research: Solid Earth, 92*(B9), 8885-8894.

Bougamont, M., Christoffersen, P., Price, S., Fricker, H. A., Tulaczyk, S., & Carter, S. P. (2015). Reactivation of Kamb Ice Stream tributaries triggers century-scale reorganization of Siple Coast ice flow in West Antarctica. *Geophysical Research Letters, 42*(20), 8471-8480.

Bougamont, M., Tulaczyk, S., & Joughin, I. (2003). Numerical investigations of the slow-down of Whillans Ice Stream, West Antarctica: is it shutting down like Ice Stream C? *Annals of Glaciology, 37*, 239-246.

Boulton, G., Caban, P., & Van Gijssel, K. (1995). Groundwater flow beneath ice sheets: Part I—Large scale patterns. *Quaternary Science Reviews, 14*(6), 545-562.

Boyce, J. I., & Eyles, N. (1991). Drumlins carved by deforming till streams below the Laurentide ice sheet. *Geology, 19*(8), 787-790.

Brennand, T. A. (2000). Deglacial meltwater drainage and glaciodynamics: inferences from Laurentide eskers, Canada. *Geomorphology, 32*(3-4), 263-293.

Brown, V. H., Stokes, C. R., & O'Cofaigh, C. (2011). The glacial geomorphology of the north-west sector of the Laurentide Ice Sheet. *Journal of Maps, 7*(1), 409-428.

Carter, S. P., Fricker, H. A., & Siegfried, M. R. (2017). Antarctic subglacial lakes drain through sediment-floored canals: theory and model testing on real and idealized domains. *The Cryosphere, 11*(1), 381-405.

Chandler, B. M., Evans, D. J., Roberts, D. H., Ewertowski, M., & Clayton, A. I. (2016). Glacial geomorphology of the Skálafellsjökull foreland, Iceland: A case study of 'annual'moraines. *Journal of Maps, 12*(5), 904-916.

Chandler, D., Wadham, J., Lis, G., Cowton, T., Sole, A., Bartholomew, I., . . . Mair, D. (2013). Evolution of the subglacial drainage system beneath the Greenland Ice Sheet revealed by tracers. *Nature Geoscience, 6*(3), 195-198.

Chandler, D. M., Wadham, J. L., Nienow, P. W., Doyle, S. H., Tedstone, A. J., Telling, J., . . . Hubbard, A. (2021). Rapid development and persistence of efficient subglacial drainage under 900 m-thick ice in Greenland. *Earth and Planetary Science Letters, 566*, 116982.

Clark, C. D. (1993). Mega-scale glacial lineations and cross-cutting ice-flow landforms. *Earth surface processes and landforms, 18*(1), 1-29.

Cowton, T., Nienow, P., Sole, A., Wadham, J., Lis, G., Bartholomew, I., . . . Chandler, D. (2013). Evolution of drainage system morphology at a land-terminating Greenlandic outlet glacier. *Journal of Geophysical Research: Earth Surface, 118*(1), 29-41.

Cuffey, K. M., & Paterson, W. S. B. (2010). *The physics of glaciers*: Academic Press.

Das, S. B., Joughin, I., Behn, M. D., Howat, I. M., King, M. A., Lizarralde, D., & Bhatia, M. P. (2008). Fracture propagation to the base of the Greenland Ice Sheet during supraglacial lake drainage. *Science, 320*(5877), 778-781.

Davison, B., Sole, A., Cowton, T., Lea, J., & Fahrner, D. (2019). *Subglacial drainage evolution modulates tidewater glacier ice flow variability.* Paper presented at the Geophysical Research Abstracts.

Davison, B., Sole, A. J., Cowton, T., Lea, J., Slater, D. A., Fahrner, D., & Nienow, P. (2020). Subglacial drainage evolution modulates seasonal ice flow variability of three tidewater glaciers in southwest Greenland. *Journal of Geophysical Research: Earth Surface, 125*(9), e2019JF005492.

Davison, B. J., Sole, A. J., Livingstone, S. J., Cowton, T. R., & Nienow, P. W. (2019). The influence of hydrology on the dynamics of land-terminating sectors of the Greenland Ice Sheet. *Frontiers in Earth Science*, 10.

Dewald, N., Livingstone, S. J., & Clark, C. D. (2022). Subglacial meltwater routes of the Fennoscandian Ice Sheet. *Journal of Maps*, 1-15.

Dowdeswell, J. A., Hamilton, G. S., & Hagen, J. O. (1991). The duration of the active phase on surge-type glaciers: contrasts between Svalbard and other regions. *Journal of Glaciology, 37*(127), 388-400.

Dyke, A. S., & Morris, T. F. (1988). Drumlin fields, dispersal trains, and ice streams in Arctic Canada. *Canadian Geographer/Le Géographe Canadien, 32*(1), 86-90.

Dyke, A. S. (2004). An outline of North American deglaciation with emphasis on central and northern Canada. *Developments in quaternary sciences, 2*, 373-424.

Dyke, A. S., Moore, A., & Robertson, L. (2003). Deglaciation of North America.

Elsworth, C. W., & Suckale, J. (2016). Rapid ice flow rearrangement induced by subglacial drainage in West Antarctica. *Geophysical Research Letters, 43*(22), 11,697-611,707.

Evans, D. J., Atkinson, N., & Phillips, E. (2020). Glacial geomorphology of the Neutral Hills Uplands, southeast Alberta, Canada: The process-form imprints of dynamic ice streams and surging ice lobes. *Geomorphology, 350*, 106910.

Evans, D. J., Ewertowski, M., Roberts, D. H., & Tomczyk, A. M. (2022). The historical emergence of a geometric and sinuous ridge network at the Hørbyebreen polythermal glacier snout, Svalbard and its use in the interpretation of ancient glacial landforms. *Geomorphology, 406*, 108213.

Evans, D. J., & Rea, B. R. (1999). Geomorphology and sedimentology of surging glaciers: a land-systems approach. *Annals of Glaciology, 28*, 75-82.

Evans, D. J., Storrar, R. D., & Rea, B. R. (2016). Crevasse-squeeze ridge corridors: diagnostic features of late-stage palaeo-ice stream activity. *Geomorphology, 258*, 40-50.

Evans, D. J., Young, N. J., & Cofaigh, C. Ó. (2014). Glacial geomorphology of terrestrial-terminating fast-flow lobes/ice stream margins in the southwest Laurentide Ice Sheet. *Geomorphology, 204*, 86-113.

Fitzpatrick, A. A., Hubbard, A., Joughin, I., Quincey, D. J., Van As, D., Mikkelsen, A. P., . . . Jones, G. A.

(2013). Ice flow dynamics and surface meltwater flux at a land-terminating sector of the Greenland ice sheet. *Journal of Glaciology, 59*(216), 687-696.

Flowers, G. E. (2015). Modelling water flow under glaciers and ice sheets. *Proceedings of the Royal Society A: Mathematical, Physical and Engineering Sciences, 471*(2176), 20140907.

Fountain, A. G., & Walder, J. S. (1998). Water flow through temperate glaciers. *Reviews of Geophysics, 36*(3), 299-328.

Fowler, A. (1987). A theory of glacier surges. *Journal of Geophysical Research: Solid Earth, 92*(B9), 9111-9120.

Fowler, A., & Johnson, C. (1996). Ice-sheet surging and ice-stream formation. *Annals of glaciology, 23*, 68-73.

Fricker, H. A., Scambos, T., Bindschadler, R., & Padman, L. (2007). An active subglacial water system in West Antarctica mapped from space. *Science, 315*(5818), 1544-1548.

Greenwood, S. L., Clark, C. D., & Hughes, A. L. (2007). Formalising an inversion methodology for reconstructing ice-sheet retreat patterns from meltwater channels: application to the British Ice Sheet. *Journal of Quaternary Science: Published for the Quaternary Research Association, 22*(6), 637-645.

Hewitt, I. J. (2011). Modelling distributed and channelized subglacial drainage: the spacing of channels. *Journal of Glaciology, 57*(202), 302-314.

Hindmarsh, R. C. (2009). Consistent generation of ice-streams via thermo-viscous instabilities modulated by membrane stresses. *Geophysical research letters, 36*(6).

Hoffman, M. J., Andrews, L. C., Price, S. F., Catania, G. A., Neumann, T. A., Lüthi, M. P., . . . Morriss, B. (2016). Greenland subglacial drainage evolution regulated by weakly connected regions of the bed. *Nature communications, 7*(1), 1-12.

Hogan, K., Arnold, N., Larter, R., Kirkham, J., Noormets, R., Ó Cofaigh, C., . . . Dowdeswell, J. (2022). Subglacial Water Flow Over an Antarctic Palaeo-Ice Stream Bed. *Journal of Geophysical Research: Earth Surface, 127*(2), e2021JF006442.

Hooke, R. L., Laumann, T., & Kohler, J. (1990). Subglacial water pressures and the shape of subglacial conduits. *Journal of Glaciology, 36*(122), 67-71.

Hulbe, C., & Fahnestock, M. (2007). Century-scale discharge stagnation and reactivation of the Ross ice streams, West Antarctica. *Journal of Geophysical Research: Earth Surface, 112*(F3).

Iken, A., & Bindschadler, R. A. (1986). Combined measurements of subglacial water pressure and surface velocity of Findelengletscher, Switzerland: conclusions about drainage system and sliding mechanism. *Journal of Glaciology, 32*(110), 101-119.

Ingólfsson, Ó., Benediktsson, Í. Ö., Schomacker, A., Kjær, K. H., Brynjólfsson, S., Jónsson, S. A., . . . Johnson, M. D. (2016). Glacial geological studies of surge-type glaciers in Iceland—Research status and future challenges. *Earth-Science Reviews, 152*, 37-69.

Jay-Allemand, M., Gillet-Chaulet, F., Gagliardini, O., & Nodet, M. (2011). Investigating changes in basal conditions of Variegated Glacier prior to and during its 1982–1983 surge. *The Cryosphere, 5*(3), 659-672.

Jennings, C. E. (2006). Terrestrial ice streams—a view from the lobe. *Geomorphology, 75*(1-2), 100-124.

Jiskoot, H., Murray, T., & Luckman, A. (2003). Surge potential and drainage-basin characteristics in East Greenland. *Annals of Glaciology, 36*, 142-148.

Joughin, I., Das, S. B., King, M. A., Smith, B. E., Howat, I. M., & Moon, T. (2008). Seasonal speedup along the western flank of the Greenland Ice Sheet. *Science, 320*(5877), 781-783.

Kamb, B. (1987). Glacier surge mechanism based on linked cavity configuration of the basal water conduit system. *Journal of Geophysical Research: Solid Earth, 92*(B9), 9083-9100.

Kamb, B., Raymond, C., Harrison, W., Engelhardt, H., Echelmeyer, K., Humphrey, N., . . . Pfeffer, T. (1985). Glacier surge mechanism: 1982-1983 surge of Variegated Glacier, Alaska. *Science, 227*(4686), 469-479.

Kehew, A. E., Nicks, L. P., & Straw, W. T. (1999). Palimpsest tunnel valleys: evidence for relative timing of advances in an interlobate area of the Laurentide ice sheet. *Annals of Glaciology, 28*, 47-52.

Kehew, A. E., Piotrowski, J. A., & Jørgensen, F. (2012). Tunnel valleys: Concepts and controversies—A review. *Earth-Science Reviews, 113*(1-2), 33-58.

Kyrke-Smith, T., Katz, R., & Fowler, A. (2014). Subglacial hydrology and the formation of ice streams. *Proceedings of the Royal Society A: Mathematical, Physical and Engineering Sciences, 470*(2161), 20130494.

Lelandais, Thomas. 2018. Modélisation analogique des écoulements d'eau sous-glaciaire : implications sur les relations entre vallées tunnels et dynamique glaciaire. Sciences de la Terre. Le Mans Université, 2018. Français. ⟨NNT : 2018LEMA1022⟩. ⟨tel-02080357⟩

Lelandais, T., Mourgues, R., Ravier, É., Pochat, S., Strzerzynski, P., & Bourgeois, O. (2016). Experimental modeling of pressurized subglacial water flow: Implications for tunnel valley formation. *Journal of Geophysical Research: Earth Surface, 121*(11), 2022-2041.

Lelandais, T., Ravier, É., Pochat, S., Bourgeois, O., Clark, C., Mourgues, R., & Strzerzynski, P. (2018). Modelled subglacial floods and tunnel valleys control the life cycle of transitory ice streams. *The Cryosphere, 12*(8), 2759-2772.

Lemmen, D. S., Duk-Rodkin, A., & Bednarski, J. M. (1994). Late glacial drainage systems along the northwestern margin of the Laurentide Ice Sheet. *Quaternary Science Reviews, 13*(9-10), 805-828.

Livingstone, S. J., Chu, W., Ely, J. C., & Kingslake, J. (2017). Paleofluvial and subglacial channel networks beneath Humboldt Glacier, Greenland. *Geology, 45*(6), 551-554.

Livingstone, S. J., Utting, D. J., Ruffell, A., Clark, C. D., Pawley, S., Atkinson, N., & Fowler, A. C. (2016). Discovery of relict subglacial lakes and their geometry and mechanism of drainage. *Nature communications, 7*(1), 1-9.

Lliboutry, L. (1968). General theory of subglacial cavitation and sliding of temperate glaciers. *Journal of Glaciology, 7*(49), 21-58.

Luckman, A., Murray, T., & Strozzi, T. (2002). Surface flow evolution throughout a glacier surge measured by satellite radar interferometry. *Geophysical research letters, 29*(23), 10-11-10-14.

Magnússon, E., Björnsson, H., Rott, H., & Pálsson, F. (2010). Reduced glacier sliding caused by persistent drainage from a subglacial lake. *The Cryosphere, 4*(1), 13-20.

Magnússon, E., Rott, H., Björnsson, H., & Pálsson, F. (2007). The impact of jökulhlaups on basal sliding observed by SAR interferometry on Vatnajökull, Iceland. *Journal of Glaciology, 53*(181), 232-240.

Margold, M., Stokes, C. R., & Clark, C. D. (2015). Ice streams in the Laurentide Ice Sheet: Identification, characteristics and comparison to modern ice sheets. *Earth-Science Reviews, 143*, 117-146.

Margold, M., Stokes, C. R., & Clark, C. D. (2018). Reconciling records of ice streaming and ice margin retreat to produce a palaeogeographic reconstruction of the deglaciation of the Laurentide Ice Sheet. *Quaternary science reviews, 189*, 1-30.

Mouginot, J., Rignot, E., Bjørk, A. A., Van den Broeke, M., Millan, R., Morlighem, M., . . . Wood, M. (2019). Forty-six years of Greenland Ice Sheet mass balance from 1972 to 2018. *Proceedings of the national academy of sciences, 116*(19), 9239-9244.

Murray, T., Strozzi, T., Luckman, A., Jiskoot, H., & Christakos, P. (2003). Is there a single surge mechanism? Contrasts in dynamics between glacier surges in Svalbard and other regions. *Journal of Geophysical Research: Solid Earth, 108*(B5).

Mäkinen, J., Kajuutti, K., Palmu, J.-P., Ojala, A., & Ahokangas, E. (2017). Triangular-shaped landforms reveal subglacial drainage routes in SW Finland. *Quaternary Science Reviews, 164*, 37-53.

Nanni, U., Gimbert, F., Roux, P., & Lecointre, A. (2021). Observing the subglacial hydrology network and its dynamics with a dense seismic array. *Proceedings of the National Academy of Sciences, 118*(28).

Nienow, P., Sole, A., Slater, D. A., & Cowton, T. (2017). Recent advances in our understanding of the role of meltwater in the Greenland Ice Sheet system. *Current Climate Change Reports, 3*(4), 330-344.

Nye, J. F. (1959). The motion of ice sheets and glaciers. *Journal of Glaciology, 3*(26), 493-507.

Nye, J. F., & Frank, F. (1973). *Hydrology of the intergranular veins in a temperate glacier.*

Paper presented at the Symposium on the Hydrology of Glaciers.

Palmer, S., Shepherd, A., Nienow, P., & Joughin, I. (2011). Seasonal speedup of the Greenland Ice Sheet linked to routing of surface water. *Earth and Planetary Science Letters, 302*(3-4), 423-428.

Paola, C., Straub, K., Mohrig, D., & Reinhardt, L. (2009). The "unreasonable effectiveness" of stratigraphic and geomorphic experiments. *Earth-Science Reviews, 97*(1-4), 1-43.

Patterson, C. J. (1997). Southern Laurentide ice lobes were created by ice streams: Des Moines Lobe in Minnesota, USA. *Sedimentary Geology, 111*(1-4), 249-261.

Payne, A., & Dongelmans, P. (1997). Self-organization in the thermomechanical flow of ice sheets. *Journal of Geophysical Research: Solid Earth, 102*(B6), 12219-12233.

Phillips, E., & Lee, J. R. (2013). Development of a subglacial drainage system and its effect on glacitectonism within the polydeformed Middle Pleistocene (Anglian) glacigenic sequence of north Norfolk, Eastern England. *Proceedings of the Geologists' Association, 124*(5), 855-875.

Pitcher, L. H., Smith, L. C., Gleason, C. J., Miège, C., Ryan, J. C., Hagedorn, B., . . . Forster, R. R. (2020). Direct observation of winter meltwater drainage from the Greenland Ice Sheet. *Geophysical Research Letters, 47*(9), e2019GL086521.

Rada, C., & Schoof, C. (2018). Channelized, distributed, and disconnected: subglacial drainage under a valley glacier in the Yukon. *The Cryosphere, 12*(8), 2609-2636.

Raymond, C. F. (1987). How do glaciers surge? A review. *Journal of Geophysical Research: Solid Earth, 92*(B9), 9121-9134.

Raymond, C., Echelmeyer, K., Whillans, I., & Doake, C. (2001). Ice stream shear margins. *The West Antarctic ice sheet: behavior and environment, 77*, 137-155.

Rignot, E., Mouginot, J., Scheuchl, B., Van Den Broeke, M., Van Wessem, M. J., & Morlighem, M. (2019). Four decades of Antarctic Ice Sheet mass balance from 1979–2017. *Proceedings of the National Academy of Sciences, 116*(4), 1095-1103.

Röthlisberger, H. (1972). Water pressure in intra-and subglacial channels. *Journal of Glaciology, 11*(62), 177-203.

Round, V., Leinss, S., Huss, M., Haemmig, C., & Hajnsek, I. (2017). Surge dynamics and lake outbursts of Kyagar Glacier, Karakoram. *The Cryosphere, 11*(2), 723-739.

Schoof, C. (2004). On the mechanics of ice-stream shear margins. *Journal of Glaciology, 50*(169), 208-218.

Sevestre, H., Benn, D. I., Luckman, A., Nuth, C., Kohler, J., Lindbäck, K., & Pettersson, R. (2018). Tidewater glacier surges initiated at the terminus. *Journal of Geophysical Research: Earth Surface, 123*(5), 1035-1051.

Sharpe, D., Lesemann, J.-E., Knight, R., & Kjarsgaard, B. (2021). Regional stagnation of the western Keewatin ice sheet and the significance of meltwater corridors and eskers, northern Canada. *Canadian Journal of Earth Sciences, 58*(10), 1005-1026.

Shreve, R. (1972). Movement of water in glaciers. *Journal of Glaciology, 11*(62), 205-214.

Siegfried, M. R., Fricker, H. A., Carter, S. P., & Tulaczyk, S. (2016). Episodic ice velocity fluctuations triggered by a subglacial flood in West Antarctica. *Geophysical Research Letters, 43*(6), 2640-2648.

Smith, D. G. (1994). Glacial Lake McConnell: paleogeography, age, duration, and associated river deltas, Mackenzie River basin, western Canada. *Quaternary Science Reviews, 13*(9-10), 829-843.

Sole, A. J., Mair, D. W. F., Nienow, P. W., Bartholomew, I., King, M., Burke, M. J., & Joughin, I. (2011). Seasonal speedup of a Greenland marine-terminating outlet glacier forced by surface melt–induced changes in subglacial hydrology. *Journal of Geophysical Research: Earth Surface, 116*(F3).

Stearns, L. A., Smith, B. E., & Hamilton, G. S. (2008). Increased flow speed on a large East Antarctic outlet glacier caused by subglacial floods. *Nature Geoscience, 1*(12), 827-831.

Stokes, C. R., & Clark, C. D. (2002). Ice stream shear margin moraines. *Earth Surface Processes and Landforms, 27*(5), 547-558.

Stokes, C., Spagnolo, M., Clark, C., Cofaigh, C. Ó., Lian, O., & Dunstone, R. (2013). Formation of mega-scale glacial lineations on the Dubawnt Lake Ice Stream bed: 1. size, shape and spacing from a large remote sensing dataset. *Quaternary Science Reviews, 77*, 190-209.

Stokes, C. R. (2018). Geomorphology under ice streams: moving from form to process. *Earth Surface Processes and Landforms, 43*(1), 85-123.

Stokes, C. R., Clark, C. D., & Storrar, R. (2009). Major changes in ice stream dynamics during deglaciation of the north-western margin of the Laurentide Ice Sheet. *Quaternary Science Reviews, 28*(7-8), 721-738.

Storrar, R. D., Stokes, C. R., & Evans, D. J. (2014). Increased channelization of subglacial drainage during deglaciation of the Laurentide Ice Sheet. *Geology, 42*(3), 239-242.

Sund, M., Lauknes, T. R., & Eiken, T. (2014). Surge dynamics in the Nathorstbreen glacier system, Svalbard. *The Cryosphere, 8*(2), 623-638.

Sundal, A. V., Shepherd, A., Nienow, P., Hanna, E., Palmer, S., & Huybrechts, P. (2011). Melt-induced speed-up of Greenland ice sheet offset by efficient subglacial drainage. *Nature, 469*(7331), 521-524.

Tedstone, A. J., Nienow, P. W., Gourmelen, N., Dehecq, A., Goldberg, D., & Hanna, E. (2015). Decadal slowdown of a land-terminating sector of the Greenland Ice Sheet despite warming. *Nature, 526*(7575), 692-695.

Tedstone, A. J., Nienow, P. W., Sole, A. J., Mair, D. W., Cowton, T. R., Bartholomew, I. D., & King, M. A. (2013). Greenland ice sheet motion insensitive to exceptional meltwater forcing. *Proceedings of the National Academy of Sciences, 110*(49), 19719-19724.

van der Vegt, P., Janszen, A., & Moscariello, A. (2012). Tunnel valleys: current knowledge and future perspectives. *Geological Society, London, Special Publications, 368*(1), 75-97.

Vérité, J., Ravier, É., Bourgeois, O., Bessin, P., Livingstone, S. J., Clark, C. D., . . . Mourgues, R. (2022). Formation of murtoos by repeated flooding of ribbed bedforms along subglacial meltwater corridors. *Geomorphology, 408*, 108248.

Vérité, J., Ravier, É., Bourgeois, O., Pochat, S., Lelandais, T., Mourgues, R., . . . Atkinson, N. (2021). Formation of ribbed bedforms below shear margins and lobes of palaeo-ice streams. *The Cryosphere, 15*(6), 2889-2916.

Vijay, S., King, M. D., Howat, I. M., Solgaard, A. M., Khan, S. A., & Noël, B. (2021). Greenland ice-sheet wide glacier classification based on two distinct seasonal ice velocity behaviors. *Journal of Glaciology, 67*(266), 1241-1248.

Walder, J. S. (1986). Hydraulics of subglacial cavities. *Journal of Glaciology, 32*(112), 439-445.

Walder, J. S., & Fowler, A. (1994). Channelized subglacial drainage over a deformable bed. *Journal of glaciology, 40*(134), 3-15.

Weertman, J. (1972). General theory of water flow at the base of a glacier or ice sheet. *Reviews of Geophysics, 10*(1), 287-333.

Yang, K., Smith, L. C., Andrews, L. C., Fettweis, X., & Li, M. (2022). Supraglacial drainage efficiency of the Greenland Ice Sheet estimated from remote sensing and climate models. *Journal of Geophysical Research: Earth Surface*, e2021JF006269.

Zemp, M., Huss, M., Thibert, E., Eckert, N., McNabb, R., Huber, J., . . . Gärtner-Roer, I. (2019). Global glacier mass changes and their contributions to sea-level rise from 1961 to 2016. *Nature, 568*(7752), 382-386.

Zheng, W., Pritchard, M. E., Willis, M. J., & Stearns, L. A. (2019). The possible transition from glacial surge to ice stream on Vavilov ice cap. *Geophysical Research Letters, 46*(23), 13892-13902.

Zwally, H. J., Abdalati, W., Herring, T., Larson, K., Saba, J., & Steffen, K. (2002). Surface melt-induced acceleration of Greenland ice-sheet flow. *Science, 297*(5579), 218-222.

1092 **Supplementary material**

1093 **Table S1.** Compilation of main experimental (type of drainage elements and fast-flow regimes)
1094 results for the 24 experiments conducted with similar initial parameters in this study.

| ***N° experiment*** | **Number of tunnel valleys** | **Number of channels** | **Surge-like flow regime** | **Stream-like flow regime** |
|---|---|---|---|---|
| **1** | 1 | 0 | X | |
| **2** | 3 | 0 | x | |
| **3** | 2 | 0 | x | |
| **4** | 1 | 6 | | x |
| **5** | 2 | 0 | x | |
| **6** | 5 | 5 | | x |
| **7** | 2 | 6 | | x |
| **8** | 1 | 2 | | x |
| **9** | 1 | 0 | x | |
| **10** | 5 | 3 | | x |
| **11** | 2 | 0 | x | |
| **12** | 3 | 1 | x | |
| **13** | 2 | 0 | x | |
| **14** | 5 | 2 | | X |
| **15** | 1 | 0 | X | |
| **16** | 1 | 0 | X | |
| **17** | 4 | 0 | X | |
| **18** | 9 | 0 | X | |
| **19** | 1 | 0 | X | |
| **20** | 2 | 0 | x | |
| **21** | 2 | 15 | | x |
| **22** | 2 | 0 | x | |
| **23** | 7 | 0 | x | |
| **24** | 2 | 0 | x | |

1095

1096

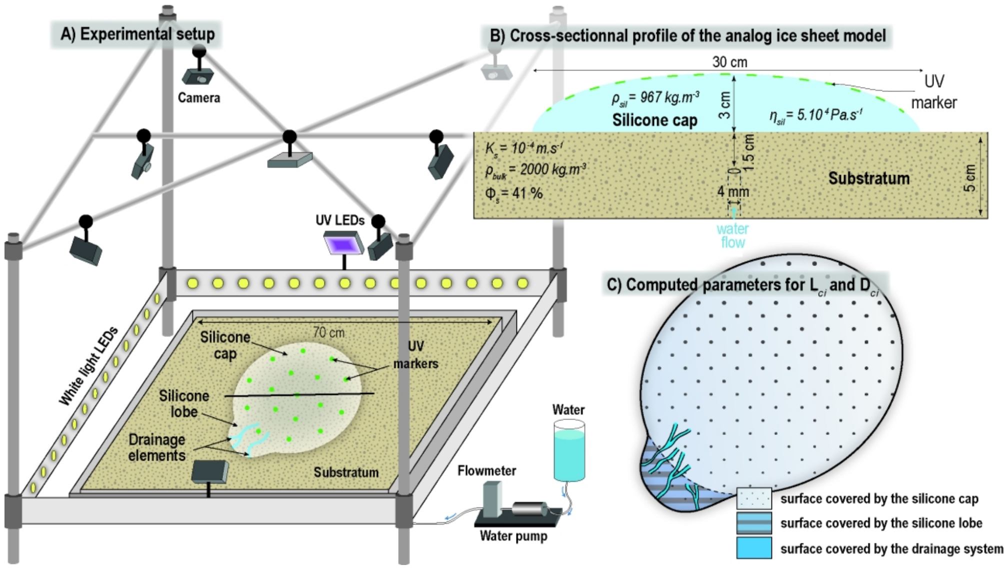


Figure 1. Description of the experimental device (after Lelandais and others, 2018) with (A) a setup overview showing the injection apparatus and the monitoring system and (B) a cross-sectional profile of the analog device displaying the position of UV markers and the physical characteristics of both the bed and the silicone cap. Parameters measured to compute the lobe cover index (Lci) and the drainage cover index (Dci) is presented in (C).

197x111mm (300 x 300 DPI)

| Water drainage characteristics | Surge-like flow regime (n= 17) | Stream-like flow regime (n= 7) |
|---|---|---|
| ***Nature of drainage elements*** | Tunnel valleys with multiple tributaries | Mainly channels with no tributaries |
| ***Distribution of drainage elements*** | Radial distribution, tunnel valleys connected to the margin | Radial distribution, channels often disconnected to the margin |
| ***Dimensions of drainage elements*** | Length average: 7.8 cm (4 cm to 15 cm)<br>Width average: 12 mm (3.5 mm to 30 mm)<br>Depth average: 0.9 mm (0.5 mm to 1.7 mm) | Length average 3.4 cm (1.8 cm to 6 cm)<br>Width average 4 mm (2 mm to 10 mm)<br>Depth average 0.4 mm (0.2 – 0.6 mm) |
| ***Morphological characteristics of drainage elements*** | U-shaped cross profile most common<br>Undulating long profile with overdeepenings and adverse slopes<br>Rectilinear, meandering or anastomosed (rare) tunnel valley system<br>Sinuosity index average: 1.15 (1 to 6) | U-shaped cross-profile most common<br>Undulating long profile with overdeepenings and adverse slopes<br>Rectilinear channels<br>Sinuosity index average: 1 |
| ***Number of drainage elements*** | Average per experiment : 2,6 (1 to 9) | Average per experiment : 8,5 (3 to 17) |
| ***Drainage cover index ($D_{ci}$)*** | 21.8 % (12.7 to 34.2) | 7.5 % (4.6 to 10.2 %) |
| ***Drainage efficicency evolution*** | Becoming efficient (after 10 to 20 minutes) | Keep inefficient throughout experiments |
| ***Drainage type*** | Well-channelised, water flow focuses in tunnel valleys | Poorly-channelised, distributed water flow (water film at the silicon-bed interface) |
| ***Formation of drainage elements*** | Tunnel valleys only formed by regressive erosion | Channels either formed by regressive or downstream erosion |
| **Silicone flow characteristics** | | |
| ***Flow velocity evolution*** | Rapid decrease of flow velocity after initial outburst flood, follows drainage efficiency evolution | Very slow decrease of flow velocity after initial outburst flood, follows drainage efficiency evolution |
| ***Final lobe cover index ($L_{ci}$)*** | 9 % (4.2 to 10.1%) | 36 % (20.3 to 54.4%) |
| ***Slicone lobe characteristics*** | Thicker lobe and steeper marginal front | Thinner lobe and smoother marginal front |
| ***Development of shear margins*** | Transitory (during surge) | Sustained |

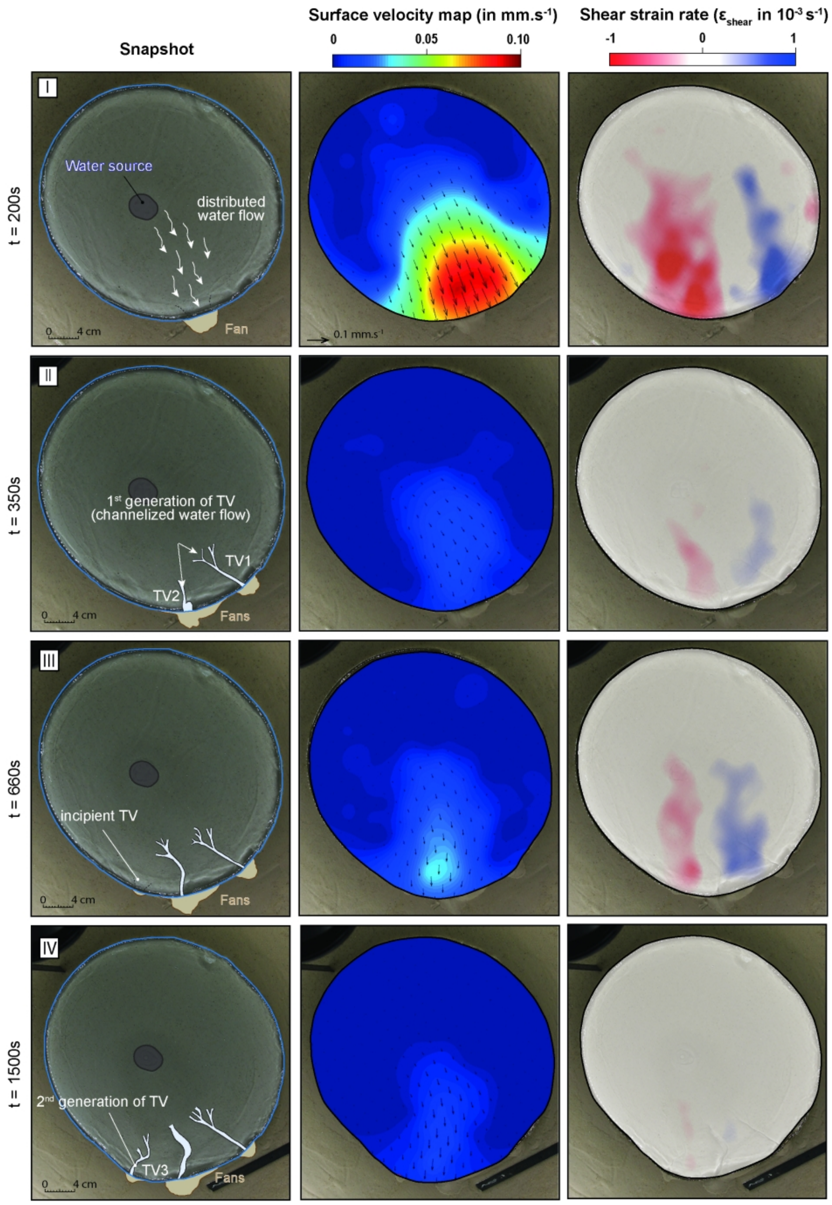


Figure 2. Typical evolution scenario for the first class of experiments (surge-like flow regime) illustrated with interpreted snapshots, surface velocity maps and surface shear strain rate maps. Stage I: silicone surge and development of shear margins coeval with the drainage of the initial water pocket. Stage II: silicone slowing during the channelization phase; formation of Tunnel Valleys (TV). Stage III: Second and minor surge, lateral migration of the fast-flowing silicone corridor and formation of a new tunnel valley. Stage IV: Silicone flow stabilisation to pre-injection velocity; shear margins vanish while tunnel valleys keep expanding.

196x285mm (300 x 300 DPI)

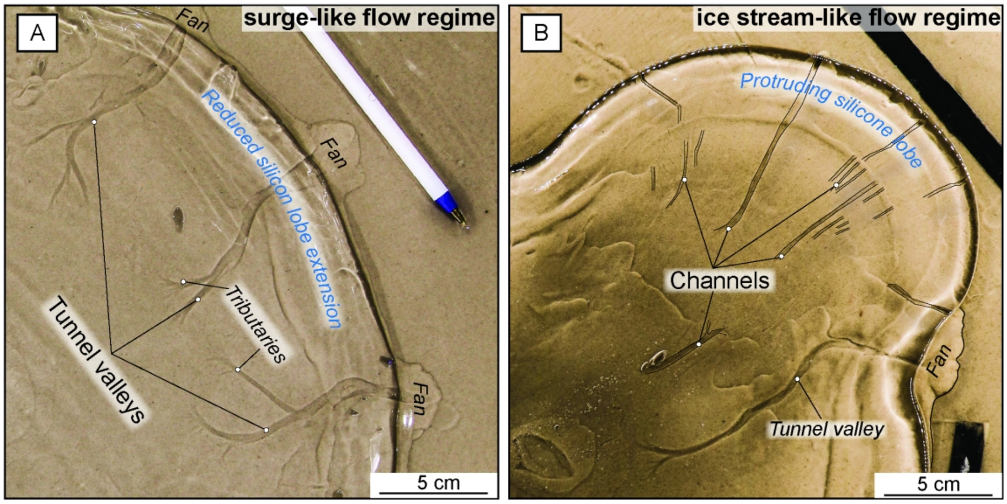


Figure 3. Snapshots of drainage features reproduced experimentally during surge-like and stream-like flow experiments. (A) Slightly sinuous tunnel valleys with tributaries connected to a silicone lobe margin typical of the surge-like flow regime scenario. (B) Multiple rectilinear channels of smaller dimensions often disconnected from margin and associated with protruding silicone lobe emerging from silicone stream. Note that the tunnel valley in panel B is becoming quickly inactive while channels keep forming.

177x88mm (300 x 300 DPI)

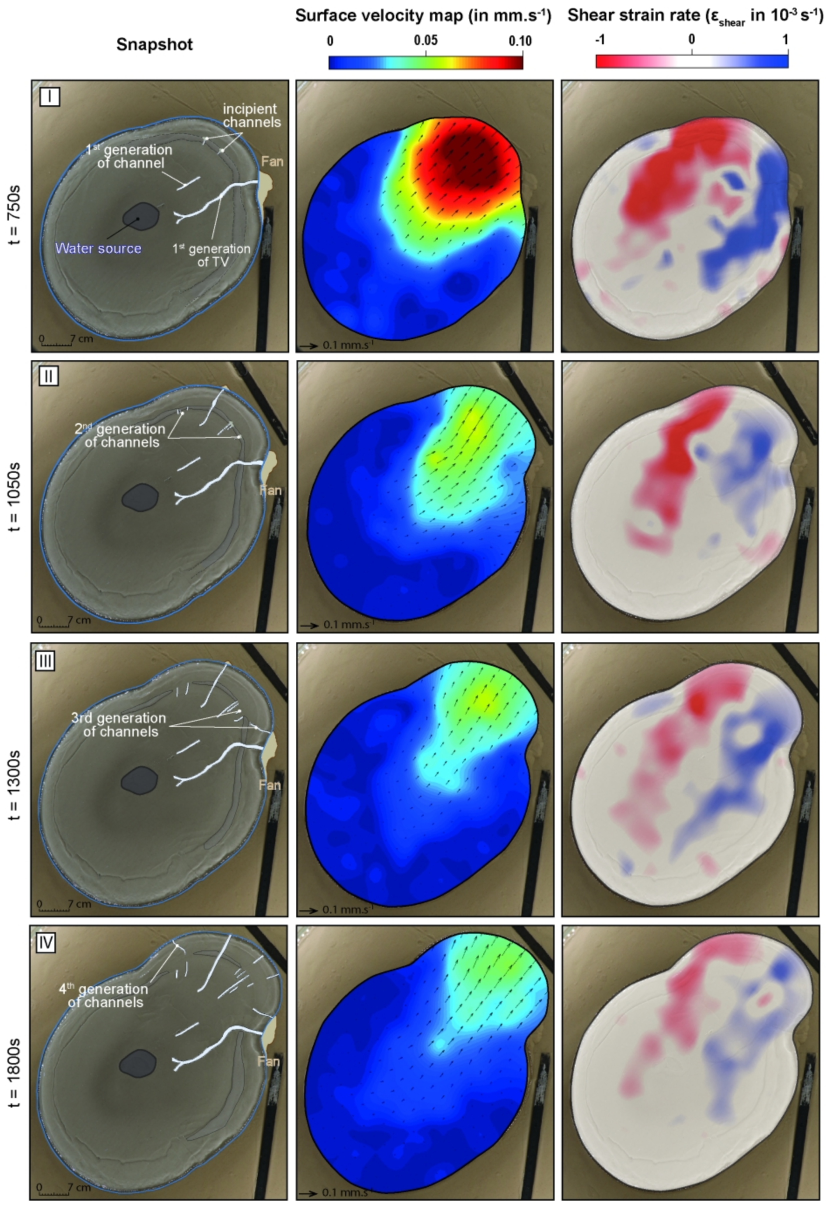


Figure 4. Evolution of the second experimental scenario (stream-like flow regime) described with interpreted snapshots, surface velocity maps and shear strain rate maps. Stage I: Sustained high silicone flow velocity (triggered during outburst flood, cf. stage I in Fig. 2) although channelization was initiated through formation of a tunnel valley. Minor channels form in parallel due to rapid cessation of the tunnel valley activity. Shear bands delineating the margin of a fast-flowing silicone corridor are observed. Stages II to IV: Tunnel valley is inactive, multiple generation of small water channels form, many of them being disconnected from the margin. The magnitude of silicone flow velocity and shear strain rates maintain at high levels throughout the experiment.

189x276mm (300 x 300 DPI)

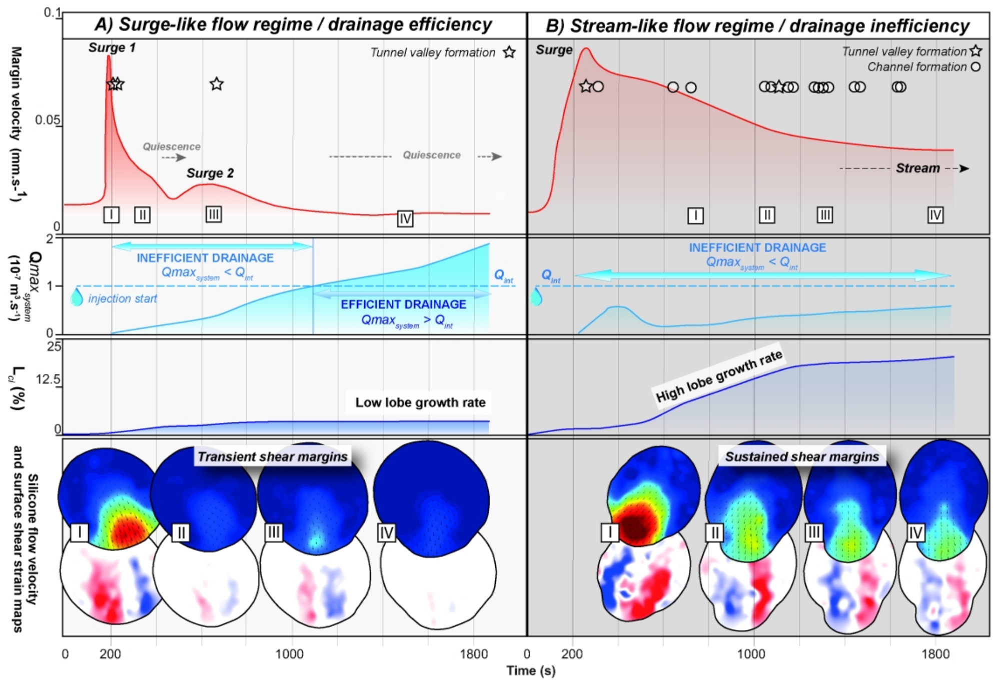


Figure 5. Monitoring of the evolution of margin velocity (in the axis of the faster flowing zone), drainage capacity of the active valley network ($Qmax_{system}$), silicone lobe cover index (Lci), flow velocity and silicone shear strain rate maps respectively for surge-like (A) and stream-like (B) flow regime experiments.

271x183mm (300 x 300 DPI)

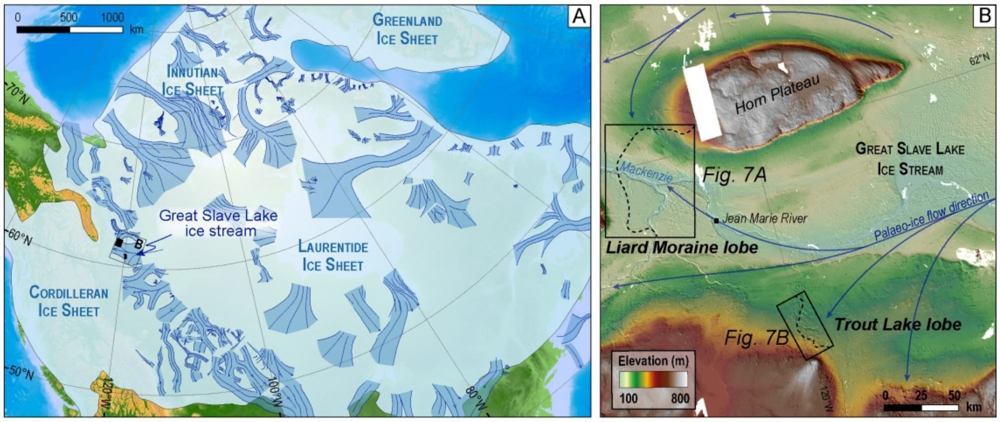


Figure 6. Geographical and palaeoglaciological context of the study area. (A) Location of the study area in the frame of the Laurentide ice sheet extent during the Last Glacial Maximum and palaeo-ice stream tracks and main flow directions (modified from Margold and others, 2018). (B) DEM of the former Great Slave Lake Ice Stream with black rectangles referring to the two palaeo-ice lobes that have been analysed in details. Dotted curved lines corresponding to former lobe position reconstructed from large end moraine complexes.

205x85mm (300 x 300 DPI)

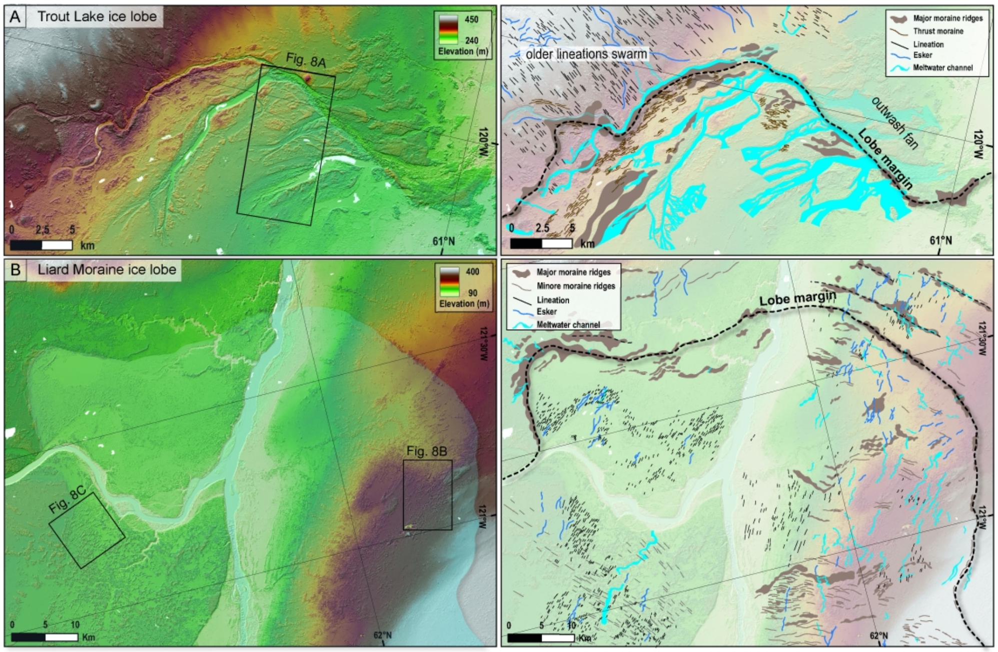


Figure 7. DEM and interpreted maps with digitized landforms of the palaeo-Trout Lake (A) and Liard moraine (B) ice lobes.

300x198mm (300 x 300 DPI)

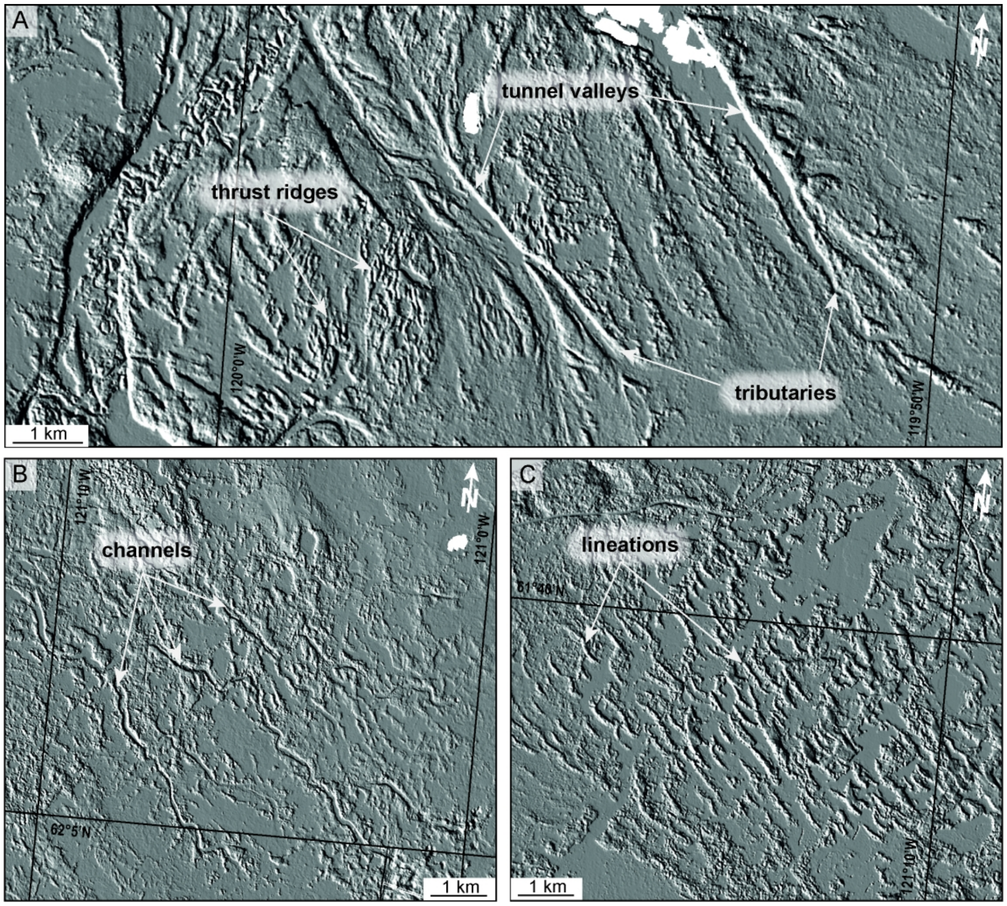


Shaded relief illustrating the drainage features and landform assemblages characterizing the bed of each palaeo-ice lobe mapped in Figure 7. (A) Large tunnel valleys with tributaries observed beneath the Trout Lake lobe. Note the occurrence of closely-spaced ridges interpreted as subglacial thrust ridges in between tunnel valleys. (B) Slightly sinuous and minor channels typically covering the bed of the Liard moraine ice lobe. (C) Lineations swarm taken from the Liard moraine ice lobe.

203x182mm (300 x 300 DPI)

| Meltwater drainage characteristics | Liard Moraine ice lobe | Trout Lake ice lobe |
|---|---|---|
| ***Nature of drainage elements*** | Channels with no tributaries and eskers, often disconnected to the ice lobe margin | Tunnel valley with multiple tributaries connected to the ice lobe margin |
| ***Distribution of drainage elements*** | Chaotic distribution of rectilinear to meandering channels | Clear radial distribution of rectilinear, meandering or braided tunnel valleys |
| ***Number of drainage elements*** | Channels: 85<br>Eskers: 142 | Tunnel valleys: 6 |
| ***Dimensions of drainage elements*** | **Channels:**<br>length average : 2942 m (± 1845m)<br>width average : 141 m (± 34m)<br>depth average : 8 m (± 4m)<br>**Eskers:**<br>length average : 1317 m (± 987m) | **Tunnel valleys:**<br>length average : 10166 m (± 4439m) width average : 446 m (± 237m) depth average : 16 m (± 10m) |
| ***Morphological characteristics of drainage elements*** | Constant width and depth<br>U-shaped (& less frequent V-shaped)<br>Flat longitudinal profile<br>Sinuosity index : 1,18 (±0,17) | Fluctuating width and depth of tunnel valleys<br>U-shaped<br>Flat longitudinal profile<br>Sinuosity index : 1,09 (±0,06) |
| ***Drainage cover index (Dci)*** | 2% | 34% |
| ***Drainage type*** | Well-channelised | Poorly-channelised |
| **Palaeo-ice lobe characteristics** | | |
| ***Ice lobe characteristics*** | Large and widespread<br>Partially constrained by topography | Small and localized<br>No topographic control |
| ***Maximum lobe dimensions ($km^2$)*** | ~ 1 800 km2 | ~ 170 km2 |
| ***Associated landforms*** | Arcuate end moraine ridges<br>Lineations | Arcuate end moraine ridges<br>Submarginal thrust masses |

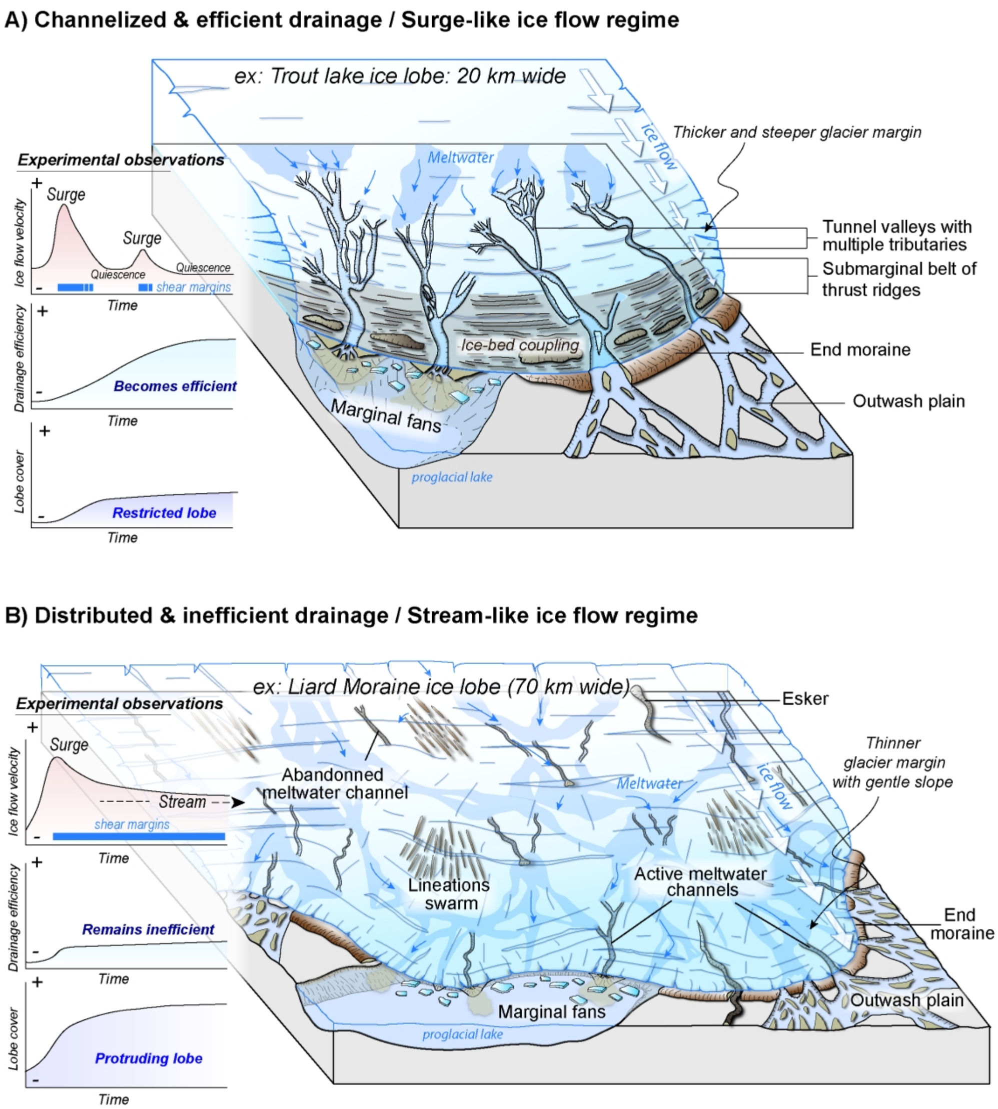


Figure 9. Idealised landsystem of channelised efficient drainage (A) and distributed inefficient drainage (B) conceptualised from experimental modelling and palaeoglaciological mapping of two ice lobes of the Great Slave Lake ice stream. The landform signature of each drainage type and ice flow regime is associated with the theoretical evolution trend of ice flow velocity, drainage efficiency and lobe spreading extrapolated from modelling results.

195x217mm (300 x 300 DPI)